

	ESA Climate Change Initiative (CCI+)	Page 1
	<b>Climate Assessment Report (CAR)</b> <b>for Climate Research Data Package 9 (CRDP#9)</b>	Version 2.1
	of the Essential Climate Variable (ECV) <b>Greenhouse Gases (GHG)</b>	6 February 2025

ESA Climate Change Initiative (CCI+)

# Climate Assessment Report (CAR)

for Climate Research Data Package No. 9 (CRDP#9)

of the Essential Climate Variable (ECV)

**Greenhouse Gases (GHG)**

**Project: GHG-CCI+**

Frédéric Chevallier<sup>a</sup> and Julia Marshall<sup>b</sup>

<sup>a</sup> Laboratoire des Sciences du Climat et de l'Environnement (LSCE), Gif-sur-Yvette, France

<sup>b</sup> Institut für Physik der Atmosphäre, Deutsches Zentrum für Luft- und Raumfahrt (DLR), Oberpfaffenhofen, Germany

	ESA Climate Change Initiative (CCI+)	Page 2
	<b>Climate Assessment Report (CAR)</b> <b>for Climate Research Data Package 9 (CRDP#9)</b>	Version 2.1
	of the Essential Climate Variable (ECV) Greenhouse Gases (GHG)	6 February 2025

### Change log:

Version Nr.	Date	Status	Reason for change
Version 1.0	8 Feb. 2024	Approved	User assessment for CRDP#8 with XCO <sub>2</sub> and XCH <sub>4</sub> products.
Version 2.0	3 Dec. 2024	Submitted	User assessment for CRDP#9 with XCO <sub>2</sub> and XCH <sub>4</sub> products.
Version 2.1	6 Feb. 2025	Approved	Correction of broken links after ESA review

This document should be cited as:

**Chevallier, F. and Marshall, J., Climate Assessment Report for Climate Research Data Package No. 9 (CRDP#9) of ESA's Climate Change Initiative project GHG-CCI+, version 2.1, 6 Feb. 2025, 2025.**

**Climate Assessment Report (CAR)**  
for Climate Research Data Package 9 (CRDP#9)

Version 2.1

of the Essential Climate Variable (ECV)  
Greenhouse Gases (GHG)

6 February 2025

## Table of contents

1. Executive summary .....	4
2. User related aspects discussed in the peer-reviewed literature .....	9
3. Assessment of satellite-derived XCO <sub>2</sub> products .....	13
3.1. Introduction .....	13
3.2. Inversion method .....	14
3.3. Global annual atmospheric growth rates .....	14
3.4. Maps of annual budgets .....	15
3.5. Annual budget time series .....	16
3.6. Fit to unassimilated upper-air measurements .....	18
3.7. Conclusions .....	19
4. Assessment of satellite-derived XCH <sub>4</sub> data products .....	21
4.1. Introduction .....	21
4.2. Preprocessing of satellite retrievals .....	22
4.2.1. Method .....	22
4.2.2. Data coverage and creation of super-observations .....	23
4.3. Methane inversion experiments with the Jena CarboScope .....	25
4.4. Global mean atmospheric mixing ratio and growth rate .....	26
4.5. Comparison of annual flux increments .....	27
4.7. Conclusions .....	31
Acknowledgements .....	33
References .....	34

	ESA Climate Change Initiative (CCI+)	Page 4
	<b>Climate Assessment Report (CAR)</b> <b>for Climate Research Data Package 9 (CRDP#9)</b>	Version 2.1
	of the Essential Climate Variable (ECV) Greenhouse Gases (GHG)	6 February 2025

## 1. Executive summary

This report describes the **assessment of the Essential Climate Variable (ECV) data products of the 9th release of the GHG-CCI Climate Research Data Package (CRDP#9)** by the Climate Research Group (CRG) of the GHG-CCI+ project (Buchwitz et al. 2015, 2017; see also GHG-CCI+ website <https://climate.esa.int/en/projects/ghgs/>). These products are CO<sub>2</sub> and CH<sub>4</sub> column retrievals (XCO<sub>2</sub> and XCH<sub>4</sub>) from current satellite instruments:

- **CO2\_OC2\_FOCA:** XCO<sub>2</sub> from NASA's OCO-2 satellite retrieved by University of Bremen using the FOCAL algorithm (global, September 2014 – February 2024, v11)
- XCO<sub>2</sub> and XCH<sub>4</sub> from Japan's GOSAT-2 satellite (products **CO2\_GO2\_SRFP**, **CH4\_GO2\_SRFP**, **CH4\_GO2\_SRPR**, global, February 2019 – December 2023, v2.0.3)
- **CH4\_S5P\_WFMD:** XCH<sub>4</sub> from the European Sentinel-5-Precursor (S5P) satellite retrieved by University of Bremen using the WFM-DOAS algorithm (global, November 2017 – December 2023, v1.8)

These products will be available via the CCI Open Data Portal (<https://climate.esa.int/en/data/#/dashboard>).

Climate researchers may find interest in these products for various reasons like evaluating climate models, estimating the uncertain parameters of these climate models, studying the variability of CO<sub>2</sub> and CH<sub>4</sub> in the atmosphere, studying wildfire or fossil fuel emission plumes, or quantifying the surface fluxes of these gases.

CRDP#9 is the fifth release of products from the GHG-CCI+ project, which started in March 2019.

Datasets CRDP#1 to CRDP#4 have been generated and released by the GHG-CCI pre-cursor project (2010 - 2018). These products are CO<sub>2</sub> and CH<sub>4</sub> products from SCIAMACHY/ENVISAT, MIPAS/ENVISAT, GOSAT, AIRS and IASI. The XCO<sub>2</sub> and XCH<sub>4</sub> and IASI products are now generated operationally via the Copernicus Climate Change Service (C3S, <https://climate.copernicus.eu/>) and are available via the Copernicus Climate Data Store (CDS, <https://cds.climate.copernicus.eu/>).

By producing retrievals of the CO<sub>2</sub> and CH<sub>4</sub> columns for these satellites and others, CRDP has given a **unique**, though heterogeneous, **climate record from space covering now more than twenty years** of the two major greenhouse gases of anthropogenic origin. **This length opens the possibility to characterize emission trends, as was already demonstrated by a series of CRDP-based studies for CH<sub>4</sub>** (e.g., Bergamaschi et al. 2013, Schneising et al., 2020) **and for CO<sub>2</sub>** (e.g., Ross et al. 2013, Schneising et al. 2013a, 2013b, Reuter et al. 2014b, Detmers et al. 2015). For the entire publication list please see <https://climate.esa.int/en/projects/ghgs/publications/>.

Previous iterations of the CRDP explored an ensemble-based approach to make use of the range of retrieval product covering several sensors and multiple retrieval algorithms (EMMA). **This ensemble**

	ESA Climate Change Initiative (CCI+)	Page 5
	<b>Climate Assessment Report (CAR)</b> <b>for Climate Research Data Package 9 (CRDP#9)</b>	Version 2.1
	of the Essential Climate Variable (ECV) Greenhouse Gases (GHG)	6 February 2025

**approach allowed for a more comprehensive assessment of the product uncertainty than just the typical uncertainty characterisation of each product through internal uncertainty propagation.**

Reuter et al. (2013, 2014a, 2020) illustrated this capability well.

The CRDP data sets, together with satellite retrievals made outside Europe, have served to **quantify regional carbon budgets** (e.g., Basu et al. 2013, Bergamaschi et al. 2013, Fraser et al. 2013, Monteil et al. 2013, Cressot et al. 2013, to cite only early ones) and more specifically (for CO<sub>2</sub>) Canada and Siberian forests (Schneising et al. 2011), Eurasia (Guerlet et al. 2013a), Tropical Asia (Basu et al. 2014), Amazonia (Parazoo et al. 2013) and Europe (Reuter et al. 2014a). However, for CO<sub>2</sub>, there remains considerable discrepancies among inversions driven by satellite retrievals, and also between these ones and bottom up estimates or inversions based on atmospheric in-situ observations (Chevallier et al. 2014a, 2019, Feng et al. 2016a, Reuter et al. 2016c). These discrepancies were also highlighted in the first eight releases of the CAR (Chevallier et al. 2013, 2015, 2016, 2017; Chevallier 2020; Chevallier and Marshall 2021, 2023, 2024). For CH<sub>4</sub> it has been early and clearly demonstrated that the SCIAMACHY retrievals and the GOSAT retrievals provide important information on regional methane emissions (e.g., Bergamaschi et al. 2013, Fraser et al. 2013, Alexe et al. 2015).

Each application of the CRDP has specific user requirements (e.g., Chevallier et al., 2014b) and it is not possible to exhaustively cover them in the CRG. Instead, the CRG has focussed on global source-sink inversion from several viewpoints.

**For CO<sub>2</sub>** and for the first time in the series of Climate Assessment Reports, a CRDP product yields global inversion results that seem realistic. This study covered the two XCO<sub>2</sub> products of CRDP#9: CO<sub>2</sub>\_OC2\_FOCA which has been retrieved from OCO-2, and CO<sub>2</sub>\_GO2\_SRFP which has been retrieved from GOSAT-2. Within the CAMS/LSCE inversion system, the CO<sub>2</sub>\_OC2\_FOCAL-driven inversion fits independent upper-air measurements as well as the official CAMS inversions and yields a global distribution of CO<sub>2</sub> sources and sinks comparable to them. Only the inversion posterior growth rate, which differs from the NOAA marine boundary layer estimate by  $0.03 \pm 0.24$  ppm/a (mean±standard deviation) over years 2015-2023, is not aligned with the CAMS standard. However, the assimilation of the CO<sub>2</sub>\_GO2\_SRFP product in the CAMS/LSCE global inversion system still infers a latitudinal distribution of CO<sub>2</sub> surface fluxes that is very different from that obtained by the assimilation of surface air-sample measurements or the assimilation of NASA's retrievals from OCO-2. We think that it is less credible because it yields a much poorer simulation of the atmospheric growth rate (with a difference to NOAA's estimate of  $-0.02 \pm 0.28$  ppm for 2020-2023).

The consistent results obtained in the CAMS inversions between the surface air-sample measurements and the ACOS retrievals demonstrates that there is no fundamental limitation in atmospheric inverse modelling (e.g., in the realism of the transport model or in the modelled error statistics) when assimilating satellite XCO<sub>2</sub> retrievals. The ACOS-driven CO<sub>2</sub> surface fluxes have actually been part of the official CAMS data portfolio since year 2019 and several ACOS-driven inversions pass the quality control of Global Carbon Project's Global Carbon Budget (Friedlingstein et al. 2023). This potential of satellite XCO<sub>2</sub> retrievals is now also confirmed by the good results

	ESA Climate Change Initiative (CCI+)	Page 6
	<b>Climate Assessment Report (CAR)</b> <b>for Climate Research Data Package 9 (CRDP#9)</b>	Version 2.1
	of the Essential Climate Variable (ECV) Greenhouse Gases (GHG)	6 February 2025

obtained with CO2\_OC2\_FOCA in this CRDP release. Interestingly, our test with the CO2\_OC2\_FOCA includes the ocean glint retrievals, while the CAMS product still blacklists NASA's ones. For CO2\_GO2\_SRFP, we note that so far GOSAT-driven inversions have not reach the quality of OCO-2 driven ones to our best knowledge, and we may meet such a limitation with GOSAT-2 as well, due to the instrument quality joined to its sampling strategy. However, even with this challenge in mind, the simulation of the atmospheric growth rate still seems to be particularly poor.

About computational effort, CO2\_OC2\_FOCA's distinct advantage compared to ACOS is its representation of multiple scattering effects in the radiative transfer in a form that is not costlier than absorption. In preparation for the Copernicus CO<sub>2</sub> Monitoring Mission that will provide even larger amount of data than OCO-2 (Pinty et al., 2017), the processing of the OCO-2 archive, which is very large by today's standards, by CO2\_OC2\_FOCA represents an important achievement. In this context and resources permitting, it would be important to document their performance in more detail in order to help prioritize future developments.

**For CH<sub>4</sub>**, the WFMD retrieval product, CH4\_S5P\_WFMD, based on TROPOMI measurements from S5P, covers the longest time period. In order to expand the scope of this assessment and provide some additional context to the results of CH4\_S5P\_WFMD, the operational S5P retrieval using the RemoTeC algorithm (v2.5.0, hereafter referred to as CH4\_S5P\_SRON) has been included in the assessment as well. Previous versions of the CAR had also included the "scientific" retrieval from SRON, which included improvements to their retrieval that had not yet been integrated into the operational product. With the current version of the operational algorithm, however, these differences are now very minor, and only the operational version of the retrieval algorithm was included in this round of the assessment.

GOSAT-2 retrievals are also now available for a period of almost five years, allowing for a more complete assessment, comparable in scope to that of the TROPOMI retrievals. For GOSAT-2, two varieties of the SRON retrieval (v2.0.3) are considered, the full-physics retrieval, hereafter referred to as CH4\_GO2\_SRFP, and the proxy retrieval, CH4\_GO2\_SRPR.

The comparison begins by comparing the XCH<sub>4</sub> products to an inversion optimized using surface-based measurements from around the world. Thanks to the ever-improving timeliness of the data set available through the cooperative ObsPack initiative, it was possible to include 76 sites in the surface-based inversion, all of which had data coverage over the majority of the simulation period (2018-2023). This is based on the standard ObsPack release 6.0 (obspack\_ch4\_1\_GLOBALVIEWplus\_v6.0\_2023-12-01, Schuldt et al., 2023), augmented with the near-real-time product for measurements in 2023 (obspack\_ch4\_1\_NRT\_v6.2\_2024-06-27, Schuldt et al., 2024). In general, satellite retrievals are available for use with much less lag time than are contemporaneous in-situ measurements.

The comparison of the surface-optimized concentration fields with the satellite products shows a systematic offset with a latitudinal dependence, attributable to errors in the transport model due to poorly represented tropopause height and stratospheric gradients. In order to not map this transport

	ESA Climate Change Initiative (CCI+)	Page 7
	<b>Climate Assessment Report (CAR)</b> <b>for Climate Research Data Package 9 (CRDP#9)</b>	Version 2.1
	of the Essential Climate Variable (ECV) Greenhouse Gases (GHG)	6 February 2025

error onto the resultant fluxes, a 2<sup>nd</sup> order polynomial correction is applied. Assessing the shape of this correction shows that the latitudinal gradients of the CH<sub>4</sub>\_S5P\_WFMD retrievals from the commissioning phase (prior to April 2018) are somewhat different than the same months in following years. After this, the shape of the bias correction is roughly stable for each month, allowing for a bias correction to be projected onto more recent satellite measurements, when surface measurements are not available as a constraint. No land-sea bias is seen in the derived bias corrections for CH<sub>4</sub>\_S5P\_WFMD and CH<sub>4</sub>\_S5P\_SRON (though the latter has few data over the oceans), and the two different GOSAT-2 retrievals (SRFP and SRPR) also result in similar curves.

Inversions were carried out using CH<sub>4</sub>\_S5P\_WFMD and CH<sub>4</sub>\_S5P\_SRON from January 2018 through December 2023. As no retrievals are available for the operational product and fewer from the WFMD retrieval during the commissioning period, results for early 2018 should not be overinterpreted. For CH<sub>4</sub>\_GO2\_SRFP and CH<sub>4</sub>\_GO2\_SRPR, inversions were carried out for five years, from January 2019 through December 2023. This is despite the fact that the data product only contains measurements from February 2019: due to a technical limitation of the inversion system, inversions must always begin in January of a given calendar year, although they can end at any point during a year.

The assimilation of the S5P retrievals in the Jena CarboScope global inversion system results in methane fluxes that are largely similar in spatial distribution to those obtained by the assimilation of surface air-sample measurements, though the fluxes from the two TROPOMI-based inversions are still more similar to each other than to the surface-constrained fluxes. The TROPOMI-based inversions see larger flux increments in the tropics vs. the extratropics. In general, the flux increments seen for the overlapping years for the GOSAT-2 and S5P retrievals agree with each other, in particular with respect to increasing fluxes over the eastern Amazon (consistent with the findings of Basso et al., 2021), eastern Africa (as in Lunt et al., 2019), and Indonesia, while decreasing emissions in boreal regions, much of China, and in higher latitudes in the Southern Hemisphere.

The resultant global mean near-surface concentrations from the TROPOMI-optimized fluxes agree very well with the in-situ-based inversion, and correlate well with the global mean concentration estimates from NOAA and WDCGG, based directly on in-situ measurements. The same cannot be said of the GOSAT-based inversions, which result in a markedly different seasonal cycle (and lower) global mean mixing near-surface mixing ratio. While the seasonal cycle and amplitude of the CH<sub>4</sub>\_GO2\_SRFP- and CH<sub>4</sub>\_GO2\_SRPR-optimized concentrations generally agree well with each other, with the mean concentration in CH<sub>4</sub>\_GO2\_SRPR being slightly higher, this changes in mid-2022, with the estimated annual growth rate for the CH<sub>4</sub>\_GO2\_SRPR dropping suddenly close to 0 ppb/year (compared to all other simulations and the NOAA marine boundary layer estimate having a growth rate of approximately 10 ppb/year from mid-2022 to mid-2023).

The concentration fields resulting from the optimized fluxes were compared to independent measurements, namely aircraft profiles and total column measurements from the TCCON network of surface-based Fourier Transform Spectrometers. These results show that that TROPOMI-based inversions agree similarly to both the aircraft data and the TCCON measurements, while the GOSAT-

	ESA Climate Change Initiative (CCI+)	Page 8
	<b>Climate Assessment Report (CAR)</b> <b>for Climate Research Data Package 9 (CRDP#9)</b>	Version 2.1
	of the Essential Climate Variable (ECV) Greenhouse Gases (GHG)	6 February 2025

2-based inversions had a low offset, and did not match the variability of the measurements as well. There was also greater disagreement at higher northern latitudes, which may be the result of the bias correction not being considered in this comparison. Both CH4\_S5P\_SRON and CH4\_S5P\_WFMD performed similarly in these comparisons, but on average the optimized fields from the CH4\_S5P\_WFMD product agreed slightly better with the evaluation data.

	ESA Climate Change Initiative (CCI+)	Page 9
	<b>Climate Assessment Report (CAR) for Climate Research Data Package 9 (CRDP#9)</b>	Version 2.1
	of the Essential Climate Variable (ECV) Greenhouse Gases (GHG)	6 February 2025

## 2. User related aspects discussed in the peer-reviewed literature

The GHG-CCI project primarily aims at bringing new knowledge about the sources and sinks of CO<sub>2</sub> and CH<sub>4</sub> based on satellite-derived data products. Since the start of Phase 1 of the GHG-CCI precursor project in 2010, this aspect has been addressed in a series of publications, which are shortly summarised in the following. They usefully provide the background for the new studies that have been performed specifically for this report and that will be described next. For a full list of publications see “Project publications” on <https://climate.esa.int/en/projects/ghgs/publications/>.

We start with the publications related to natural CO<sub>2</sub> fluxes.

- Using global GOSAT XCO<sub>2</sub> retrievals, Basu et al. (2013) presented first global CO<sub>2</sub> surface flux inverse modelling results for various regions. Their analysis suggested a reduced global land sink and a shift of the carbon uptake from the tropics to the extra-tropics. In particular, their results suggested that Europe is a stronger carbon sink than expected, but this feature was not further discussed in this paper.
- Chevallier et al. (2014a) analysed an ensemble of global inversion results assimilating two GOSAT XCO<sub>2</sub> retrieval products. They found hemispheric and regional differences in posterior flux estimates that are beyond 1 sigma uncertainties. They too found a significantly larger European carbon sink or a larger North African emission than expected. They concluded to the existence of significant flaws in all main components of the inversions: the transport model, the prior error statistics and the retrievals.
- Houweling et al. (2015) presented the outcome of a large inverse modelling intercomparison experiment on the use of GOSAT retrievals. The ensemble of results confirmed the large latitudinal shift in carbon uptake, but they showed that the reduced gradient degrades the agreement with background aircraft and surface measurements.
- Reuter et al. (2014a) investigated the European carbon sink further with another ensemble of GOSAT XCO<sub>2</sub> products, a SCIAMACHY XCO<sub>2</sub> product and a new inversion method which is less sensitive to some of the issues discussed in Chevallier et al. (2014a). Reuter et al. (2014a) only used satellite XCO<sub>2</sub> retrievals over Europe to rule out that non-European satellite data adversely influence the European results and they also only used short-term (days) transport modelling to avoid long-range transport errors. Based on an extensive analysis they concluded: “We show that the satellite-derived European terrestrial carbon sink is indeed much larger ( $1.02 \pm 0.30$  GtC/year in 2010) than previously expected”. The value they derived is significantly larger compared to bottom-up estimates (not based on atmospheric measurements) of  $0.235 \pm 0.05$  GtC/year for 2001-2004 (Schulze et al, 2009).
- The findings of Reuter et al. (2014a) stimulated additional research (Feng et al. 2016a, Reuter et al. 2016c).
- Detmers et al. (2015) analyzed GOSAT XCO<sub>2</sub> retrievals to detect and quantify anomalously large carbon uptake in Australia during a strong La Niña episode.
- For flux inversions, not only the retrieved greenhouse gas values are relevant, but also their error statistics, in particular the reported uncertainties. Chevallier and O’Dell (2013) analyzed this aspect in the context of CO<sub>2</sub> flux inversions using GOSAT XCO<sub>2</sub> retrievals. For CH<sub>4</sub>, Cressot et al. (2013, 2016) studied the uncertainty of flux inversions assimilating SCIAMACHY, GOSAT or IASI XCH<sub>4</sub> retrievals.
- Focussing on Canadian and Siberian boreal forests, Schneising et al. (2011) computed longitudinal XCO<sub>2</sub> gradients from SCIAMACHY XCO<sub>2</sub> retrievals during the vegetation growing season over Canadian and Siberian boreal forests and compared the gradients with outputs from NOAA’s CO<sub>2</sub> assimilation system CarbonTracker (Peters et al. 2007). They found good agreement for the total

**Climate Assessment Report (CAR)  
for Climate Research Data Package 9 (CRDP#9)**

Version 2.1

of the Essential Climate Variable (ECV)  
Greenhouse Gases (GHG)

6 February 2025

boreal region and for inter-annual variations. For the individual regions, however, they found systematic differences suggesting a stronger Canadian boreal forest growing season CO<sub>2</sub> uptake and a weaker Siberian forest uptake compared to CarbonTracker.

- Focussing on hemispheric data and on carbon-climate feedbacks, Schneising et al. (2014a) used SCIAMACHY XCO<sub>2</sub> to study aspects related to the terrestrial carbon sink by looking at co-variations of XCO<sub>2</sub> growth rates and seasonal cycle amplitudes with near-surface temperature. They found XCO<sub>2</sub> growth rate changes of  $1.25 \pm 0.32$  ppm/year/K (approximately  $2.7 \pm 0.7$  GtC/year/K; indicating less carbon uptake in warmer years, i.e., a positive carbon-climate feedback) for the Northern Hemisphere in good agreement with CarbonTracker.
- Reuter et al. (2013) computed CO<sub>2</sub> seasonal cycle amplitudes using various satellite XCO<sub>2</sub> data products (using GHG-CCI products but also GOSAT XCO<sub>2</sub> products generated in Japan at NIES (Yoshida et al. 2013, Oshchepkov et al. 2013) and the NASA ACOS product (O'Dell et al. 2012) and compared the amplitudes with TCCON and CarbonTracker. They found that the satellite products typically agree well with TCCON but they found significantly lower amplitudes for CarbonTracker suggesting that CarbonTracker underestimates the CO<sub>2</sub> seasonal cycle amplitude by approx.  $1.5 \pm 0.5$  ppm (see also Buchwitz et al., 2015, for a discussion of these findings).
- Lindquist et al. (2015) compared satellite XCO<sub>2</sub> retrievals, surface XCO<sub>2</sub> retrievals and atmospheric model simulations in terms of XCO<sub>2</sub> seasonal cycle. They found that the satellite retrieval algorithms performed qualitatively similarly but showed notable scatter at most validation sites. None of the tested algorithm clearly outperformed another. They showed that the XCO<sub>2</sub> seasonal cycle depends on longitude especially at the mid-latitudes, which was only partially shown by the models. They also found that model-to-model differences could be larger than GOSAT-to-model differences.
- Guerlet et al. (2013a) analyzed GOSAT XCO<sub>2</sub> retrievals focusing on the Northern Hemisphere. They identified a reduced carbon uptake in the summer of 2010 and found that this is most likely due to the heat wave in Eurasia driving biospheric fluxes and fire emissions. Using a joint inversion of GOSAT and surface data, they estimated an integrated biospheric and fire emission anomaly in April–September of  $0.89 \pm 0.20$  PgC over Eurasia. They found that inversions of surface measurements alone fail to replicate the observed XCO<sub>2</sub> inter-annual variability (IAV) and underestimate emission IAV over Eurasia. They highlighted the value of GOSAT XCO<sub>2</sub> in constraining the response of land-atmosphere exchange of CO<sub>2</sub> to climate events.
- Basu et al. (2014) studied seasonal variation of CO<sub>2</sub> fluxes during 2009–2011 over Tropical Asia using GOSAT, CONTRAIL and IASI data. They found an enhanced source for 2010 and concluded that this is likely due to biosphere response to above-average temperatures in 2010 and unlikely due to biomass burning emissions.
- Parazoo et al. (2013) used GOSAT XCO<sub>2</sub> and solar induced chlorophyll fluorescence (SIF) retrievals to better understand the carbon balance of southern Amazonia.
- Ross et al. (2013) used GOSAT data to obtain information on wildfire CH<sub>4</sub>:CO<sub>2</sub> emission ratios.
- The strong El Niño event of 2015–2016, shortly after the launch of OCO-2, provided an opportunity to assess the carbon-climate feedbacks using satellite data, e.g. Liu et al. (2017) and Chatterjee et al. (2017).

Despite the fact that none of the existing satellite missions has been optimized to obtain information on anthropogenic CO<sub>2</sub> emissions, this important aspect has been addressed in several recent publications using existing satellite XCO<sub>2</sub> products.

- Schneising et al. (2013) presented an assessment of the satellite data over major anthropogenic CO<sub>2</sub> source regions. They used a multi-year SCIAMACHY XCO<sub>2</sub> data set and compared the regional XCO<sub>2</sub>

**Climate Assessment Report (CAR)  
for Climate Research Data Package 9 (CRDP#9)**

Version 2.1

of the Essential Climate Variable (ECV)  
Greenhouse Gases (GHG)

6 February 2025

enhancements and trends with the emission inventory EDGAR v4.2 (Olivier et al. 2012). They found no significant trend for the Rhine-Ruhr area in central Europe and the US East Coast but a significant increasing trend for the Yangtze River Delta in China of about  $13 \pm 8\%$ /year, in agreement with EDGAR ( $10 \pm 1\%$ /year).

- Reuter et al. (2014b) studied co-located SCIAMACHY XCO<sub>2</sub> and NO<sub>2</sub> retrievals over major anthropogenic source regions. For East Asia they found increasing emissions of NO<sub>x</sub> (+5.8%/year) and CO<sub>2</sub> (+9.8%/year), i.e., decreasing emissions of NO<sub>x</sub> relative to CO<sub>2</sub> indicating that the recently installed and renewed technology in East Asia, such as power plants and transportation, is cleaner in terms of NO<sub>x</sub> emissions than the old infrastructure, and roughly matches relative emission levels in North America and Europe.
- The higher resolution and continuous (if narrow) swath of OCO-2 has also enabled a range of plume inversion studies, focussed on the estimation of point source emissions of CO<sub>2</sub>, e.g. Nassar et al. (2017), which have been extended to make use of co-located measurements of NO<sub>2</sub> from TROPOMI by Reuter et al. (2019) and Fuentes Andrade et al. (2023).
- Byrne et al. (2023) presented an ensemble-based product estimating national CO<sub>2</sub> budgets from 2015-2020 based on OCO-2 retrievals, in support of the Global Stocktake. This built upon a previous OCO-2 inversion intercomparison study by Crowell et al. (2019).

A series of studies have also addressed methane emissions.

- SCIAMACHY data have already been extensively used to improve our knowledge on regional methane emissions prior to the start of the GHG-CCI project (e.g., Bergamaschi et al. 2009). A more recent research focus was to shed light on the unexpected renewed atmospheric methane increase during 2007 and later years using ground-based and satellite data (e.g., Rigby et al. 2008, Dlugokencky et al. 2009, Bergamaschi et al. 2009, 2013, Schneising et al. 2011, Frankenberg et al. 2011, Sussmann et al. 2012, Crevoisier et al. 2013). Based on an analysis of SCIAMACHY year 2003-2009 retrievals an increase of 7-9 ppb/year (0.4-0.5%/year) has been found with the largest increases in the tropics and northern mid latitudes (Schneising et al. 2011) but a particular region responsible for the increase has not been identified (Schneising et al. 2011; Frankenberg et al. 2011). Bergamaschi et al. (2013) used SCIAMACHY retrievals and NOAA surface data for 2003-2010 and inverse modelling in order to attribute the observed increase of atmospheric concentrations to changes in emissions. They concluded that most of this increase is due to emissions in the Tropics and the mid-latitudes of the northern hemisphere, while no significant trend was derived for Arctic latitudes. The increase is mainly attributed to anthropogenic sources, superimposed with significant inter-annual variations of emissions from wetlands and biomass burning.
- The SCIAMACHY XCH<sub>4</sub> retrievals have also been used to improve chemistry-climate models (Shindell et al. 2013, Hayman et al. 2014).
- Methane emissions have also been obtained from GOSAT, as presented in a number of publications as shown in, e.g., Fraser et al. (2013, 2014), Monteil et al. (2013), Cressot et al. (2014), Alexe et al. (2015), Turner et al. (2015) and Pandey et al. (2016). Note that for these studies, often CH<sub>4</sub> retrievals from several satellites have been used (as well as NOAA data), e.g., Monteil et al. (2013), and Alexe et al. (2015) used SCIAMACHY and GOSAT retrievals and Cressot et al. (2014, 2016) used GOSAT, SCIAMACHY and IASI. Alexe et al. (2015) showed that the different satellite products resulted in relatively consistent spatial flux adjustment patterns, particularly across equatorial

**Climate Assessment Report (CAR)  
for Climate Research Data Package 9 (CRDP#9)**of the Essential Climate Variable (ECV)  
Greenhouse Gases (GHG)

Africa and North America. Over North America, the satellite inversions result in a significant redistribution of emissions from North-East to South-Central USA, most likely due to natural gas production facilities.

- Several publications focused on (relatively localized) methane sources in the United States: For example, Schneising et al. (2014b) analyzed SCIAMACHY data over major US “fracking” areas and quantified methane emissions and leakage rates. For two of the fastest growing production regions in the US, the Bakken and Eagle Ford formations, they estimated that emissions increased by  $990 \pm 650$  ktCH<sub>4</sub>/year and  $530 \pm 330$  ktCH<sub>4</sub>/year between the periods 2006–2008 and 2009–2011. Relative to the respective increases in oil and gas production, these emission estimates correspond to leakages of  $10.1\% \pm 7.3\%$  and  $9.1\% \pm 6.2\%$  in terms of energy content, calling immediate climate benefit into question and indicating that current inventories likely underestimate the fugitive emissions from Bakken and Eagle Ford. Others also used SCIAMACHY data over the US to identify and quantify localized anthropogenic methane emission sources (Kort et al. 2014, Wecht et al. 2014). Last, Turner et al. (2015) used GOSAT retrievals within a meso-scale inversion system for the US.
- Such regional studies have been extended and expanded with the capabilities of TROPOMI, including studies focussing on basin-level oil and gas emissions of methane, including Schneising et al. (2020), and Zhang et al. (2020). This approach has been operationalized to provide weekly basin-level monitoring with the recent work of Varon et al. (2023).
- TROPOMI has also been used in recent studies to estimate national emissions, such as from China (Chen et al., 2022), and countries around the world (Shen et al., 2023).
- Recent publications have focussed on natural emissions from the Tropics using GOSAT data, such as Parker et al. (2018), Lunt et al. (2019), Feng et al. (2022), and Yin et al. (2021), finding variability in Tropical emissions to be a driver of the recent methane growth rate.
- Many recent studies have exploited the high spatial resolution and broad coverage of TROPOMI measurements to identify and estimate the emissions from point source emissions of methane. A selection of such publications includes: Maasackers et al. (2022), focussing on landfill emissions; Gao et al. (2023), assessing onshore oil and gas emissions; Lauvaux et al. (2022), focussing on oil and gas emissions; Maasackers et al. (2021), quantifying emissions from a blow-out; in this context see also Schuit et al. (2023) and Vanselow et al. (2024).
- Machine-learning methods have recently been applied by Balasus et al. (2023) to create a blended GOSAT+TROPOMI product, using the joint information to correct for retrieval biases.
- Regional inversions focussing on Eastern Asia by Liang et al. (2023) have found that inversions based on TROPOMI vs GOSAT data disagree on the distribution and magnitude of emissions across the region. Some of this difference is attributable to the difference in data coverage, with GOSAT measurements being comparatively sparse, but the lower methane emissions from the GOSAT inversions were also more consistent with surface- and aircraft-based inversions, suggesting some incongruity in the information between the two sensors.

For additional publications, see the publication list provided by the GHG-CCI+ website (<https://climate.esa.int/en/projects/ghgs/publications/>).

### 3. Assessment of satellite-derived XCO<sub>2</sub> products

#### 3.1. Introduction

Given a decade of global inverse modelling studies assimilating real XCO<sub>2</sub> retrievals (since Basu et al., 2013, see Section 2), extended to two decades in the case of partial column CO<sub>2</sub> retrievals (Chevallier et al., 2005), the current interest in XCO<sub>2</sub> products for global inverse modelling is about accurate multi-year global products. This has not been always the case (Chevallier et al, 2011). The first four GHG-CCI Climate Research Data Packages fulfilled this ambition with SCIAMACHY and TANSO retrievals.

The 5<sup>th</sup>, 6<sup>th</sup>, 7<sup>th</sup>, 8<sup>th</sup> and 9<sup>th</sup> GHG-CCI+ Climate Research Data Packages (CRDP#5, #6, #7, #8 and #9) include three XCO<sub>2</sub> products from more recent satellite instruments with a similar ambition:

- CO2\_TAN\_OCFP (not updated in CRDP#8 and #9): retrieved from TanSat using University of Leicester's UoL-FP (or OCFP) algorithm
- CO2\_OC2\_FOCA: retrieved from OCO-2 using University of Bremen's FOCAL algorithm
- CO2\_GO2\_SRF: retrieved from GOSAT-2 using SRON's RemoTeC (or SRF) algorithm

The CRDP#9 version of the last two products is evaluated in this chapter within an inverse modelling framework. The first product, CO2\_TAN\_OCFP, has not been updated since CRDP#7. Comparisons are made with the surface air-sample-driven inversion and the satellite-driven inversion of the Copernicus Atmosphere Monitoring Service (<https://atmosphere.copernicus.eu/>, Chevallier, 2023, 2024). The latter assimilated latest version 11.1 of the official bias-corrected XCO<sub>2</sub> retrievals made by the NASA Atmospheric CO<sub>2</sub> Observations from Space (ACOS) algorithm described by Osterman et al. (2022).

The evaluated product from CRDP#9 is summarized in Table 1 below. The two CRDP#9 official bias-corrected products have been processed by LSCE on a GPU (Graphics Processing Unit) partition of the supercomputer Irene.

Product ID	Satellite	Algorithm	Data provider	Reference	Period available	Evaluators (sections)
CO2_OC2_FOCA	OCO-2	FOCAL, v11	IUP, Univ. Bremen	Reuter et al., 2017a, 2017b	09/2014-02/2024	LSCE (3.2 – 3.7)
CO2_GO2_SRF	GOSAT-2	SRFP, v2.0.3	SRON	Krisna et al., 2022a	02/2019-12/2023	LSCE (3.2 – 3.7)

Table 1. XCO<sub>2</sub> products evaluated in this report.

	ESA Climate Change Initiative (CCI+)	Page 14
	<b>Climate Assessment Report (CAR)</b> for Climate Research Data Package 9 (CRDP#9)	Version 2.1
	of the Essential Climate Variable (ECV) Greenhouse Gases (GHG)	6 February 2025

### 3.2. Inversion method

The satellite data are assimilated alone, without combining them with other observations, in order to focus on their own signals. The much higher spatial resolution of the CO<sub>2</sub>\_OC2\_FOCA retrievals than the LMDz atmospheric transport model used here may cause numerical artifacts: to avoid them, we follow Crowell et al. (2019) by aggregating these retrievals in 10-second intervals, that roughly correspond to boxes of 67×10 km<sup>2</sup> for OCO-2, a surface area which is still smaller than the individual hexagon cells of size about 90 km of the model. This approach was also used in the CAMS OCO-2-driven inversion FT24r1 used here.

We use the two CRDP#9 XCO<sub>2</sub> products candidly, i.e. without modifying the retrieval values and their associated uncertainty in input to the inversion or, for CO<sub>2</sub>\_OC2\_FOCA, to the 10-s binning algorithm. We use the retrieval averaging kernels and prior profiles when assimilating them. As an example, processing the full multi-year series of CO<sub>2</sub>\_OC2\_FOCA within the inverse system required 20 days of computation on 11 GPUs.

The fluxes inferred from CO<sub>2</sub>\_OC2\_FOCA and CO<sub>2</sub>\_GO2\_SRF are compared to two benchmark inversion: the CAMS official inversion products v22r1 that exclusively assimilated surface air-sample measurements at 159 sites from the Global Atmosphere Watch programme, and the CAMS official inversion product FT24r1 that exclusively assimilated the ACOS OCO-2 v11.1 retrievals over land. Ocean glint retrievals were not assimilated in FT24r1 because of likely systematic errors (Chevallier et al., 2019), but such a selection is not done for the CRDP#9 products here in the absence of similar evidence. Actually, for CRDP#7, we made a test without the ocean data of CO<sub>2</sub>\_OC2\_FOCA, but results were found less realistic than with these (Chevallier and Marshall, 2023).

The inversion system works at the grid-point weekly scale and generates a large volume of data. The present comparison focuses on a few key quantities: (i) the global annual growth rate that is well known from the NOAA marine surface data (Conway et al. 1994, <https://gml.noaa.gov/ccgg/trends/global.html>), (ii) the grid-point annual-total fluxes, (iii) zonal annual CO<sub>2</sub> budgets, (iv) the model-equivalent to upper-air measurements.

### 3.3. Global annual atmospheric growth rates

In 2019, the Inverse modelling protocol for the annual global carbon budget of the Global Carbon Project (GCP) started to use a quality criterion on the global annual atmospheric growth rate of the inversion (Chevallier et al. 2019, 2020, 2021, 2022, 2023): “using a conversion factor, the series of annual fluxes will be compared to the annual trend of globally-averaged marine measurements (<https://gml.noaa.gov/ccgg/trends/global.html>). Submissions that show notably different interannual variations will be excluded.”

The OCO-2 Science team's Model Intercomparison Project v10 (MIPv10) adopted a selection criterion on the mean growth rate for the inversion products it gathered for the Global Stocktake (Byrne et al., 2023): it required the selected inversions to have a 6-year growth rate over 2015-2020 equal to 2.54

	ESA Climate Change Initiative (CCI+)	Page 15
	<b>Climate Assessment Report (CAR)</b> <b>for Climate Research Data Package 9 (CRDP#9)</b>	Version 2.1
	of the Essential Climate Variable (ECV) Greenhouse Gases (GHG)	6 February 2025

$\pm 0.08$  ppm/a, based on NOAA's reference estimate (Brendan Byrne, personal communication, 4 January 2022). This criterion is quantitative, in contrast to the GCP one, but it is limited to the mean value: it just checks that the model simulation does not diverge over time.

In all previous CARs, poor inversion results were associated to poor inversion annual growth rates in terms of bias and/or standard deviation.

Over the nine full years 2015-2023, the CAMS satellite inversion FT24r1 fits NOAA's numbers (as of 5 October 2024) with a bias of  $-0.03$  ppm/a and a standard deviation of  $0.13$  ppm/a <sup>1</sup>. Its surface-driven counterpart (v22r1) shows a smaller bias and a larger standard deviation:  $0.01 \pm 0.14$  ppm/a <sup>2</sup>. The FOCAL-driven inversion is at  $0.03 \pm 0.24$  ppm/a. The fit is better than with the FOCAL version of the previous CRDP ( $0.00 \pm 0.28$  ppm for 2015-2021 in CRDP#8 vs.  $+0.02 \pm 0.20$  ppm here for the same period). With a mean growth rate over 2015-2020 equal to  $2.56$  ppm/a, the FOCAL inversion passes the MIPv10 6-year growth-rate criterion, like the CAMS satellite inversion FT24r1 (with a value of  $2.50$  ppm/a).

For the SRFP-driven inversion, we consider the four full years 2020 – 2023, knowing that the retrieval product does not allow any spin-down for the fourth one, and we find a bias of  $-0.02$  ppm/a and a standard deviation of  $0.28$  ppm/a.

### 3.4. Maps of annual budgets

Figure 1 display the maps of the inferred annual budgets of natural CO<sub>2</sub> fluxes for year 2020 that is included in the two CRDP products considered here. The figures also display the maps for the two CAMS inversions. As shown already by Chevallier et al. (2019), the two CAMS inversions have comparable flux patterns in the northern extra-Tropics, but the ACOS-driven inversion has more spatial gradients than the surface-driven one in the Tropical lands where the surface measurement network is particularly sparse. The two CRDP#9-driven inversions have even larger gradients there (Australia excepted), but also in the northern extra-Tropics. The colour bar has actually not been adapted to their variability. Surprisingly, many spatial patterns (irrespective of their amplitude) are similar between the three satellite-driven inversions over land, in particular between the two OCO-2 ones. Over the ocean, the four inversions display comparable patterns. None of the maps seems unrealistic here, which was not the case before CRDP#8 (Chevallier and Marshall, 2023).

<sup>1</sup> We assume a conversion factor of  $2.086$  GtC·ppm<sup>-1</sup>, from Prather (2012), which may be slightly different from other studies.

<sup>2</sup> Note that the NOAA estimate and the surface-driven CAMS one are not independent since the surface-driven CAMS inversion assimilates the individual NOAA measurements

**Climate Assessment Report (CAR)  
for Climate Research Data Package 9 (CRDP#9)**

Version 2.1

of the Essential Climate Variable (ECV)  
Greenhouse Gases (GHG)

6 February 2025

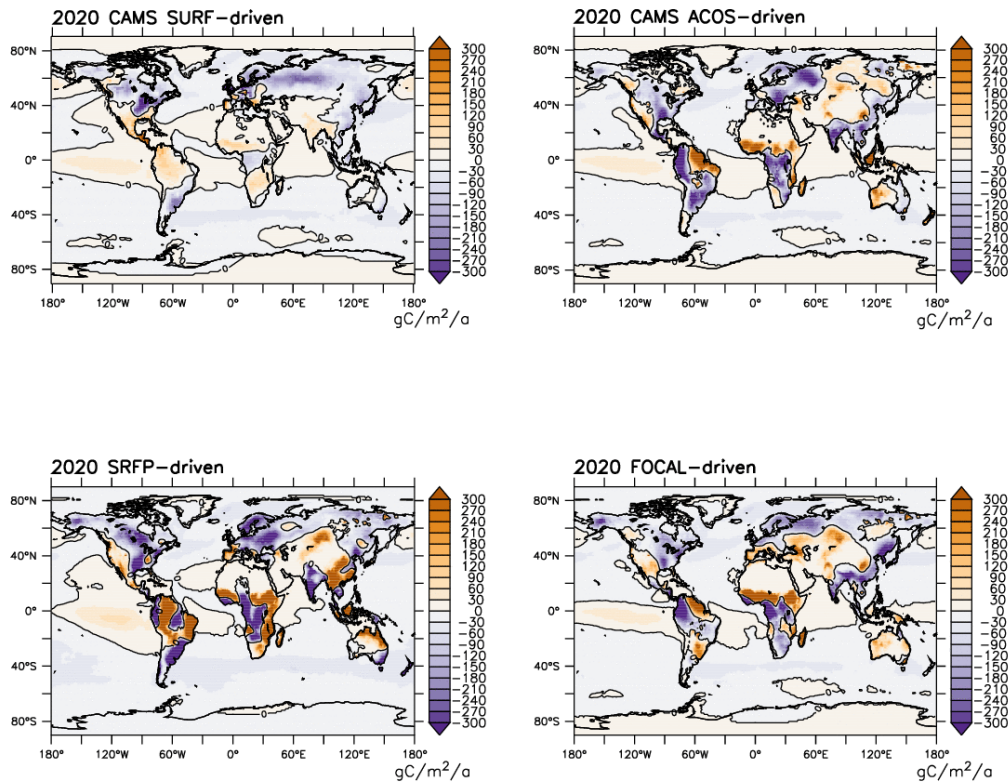


Figure 1. Grid-point annual budget of the natural CO<sub>2</sub> fluxes for year 2020, for the two CAMS inversions, for the FOCAL inversion and for the SRFP inversion. In the sign convention, positive fluxes correspond to a net carbon source into the atmosphere.

### 3.5. Annual budget time series

The time series of the annual natural carbon budgets at several very broad scales are displayed in Figure 2 for the period between 2015 and 2023 for the two CAMS inversions and the two CRDP#9 ones: the globe, the northern or southern extra-Tropics, and the Tropics with lands and oceans either separated or combined. At the global scale (top row), the curves reflect the growth rate discussed in Section 3.3, but without the fossil fuel and cement flux component. The CAMS ACOS inversion remains close to the CAMS surface inversion in all subplots, which is not the case for the CO<sub>2</sub>\_GO<sub>2</sub>\_SRFP inversion. The CO<sub>2</sub>\_O<sub>2</sub>\_FOCA is not far, in contrast to the previous CRDP releases.

The two CAMS inversions and the CO<sub>2</sub>\_OC<sub>2</sub>\_FOCA one locate the land sink mostly in the northern extra-Tropics in contrast to the CO<sub>2</sub>\_GO<sub>2</sub>\_SRFP one that locates it mostly in the southern extra-Tropics despite its relatively small surface area (middle row). In all four inversions, a large year-to-year variability is seen in the Tropics.



### Climate Assessment Report (CAR) for Climate Research Data Package 9 (CRDP#9)

of the Essential Climate Variable (ECV)  
Greenhouse Gases (GHG)

The ocean sink latitudinal distribution inferred from the two CAMS inversions and the CO2\_OC2\_FOCA one is comparable but the CO2\_GO2\_SRFP one infers a much larger sink close to 4 GtC/a (bottom row).

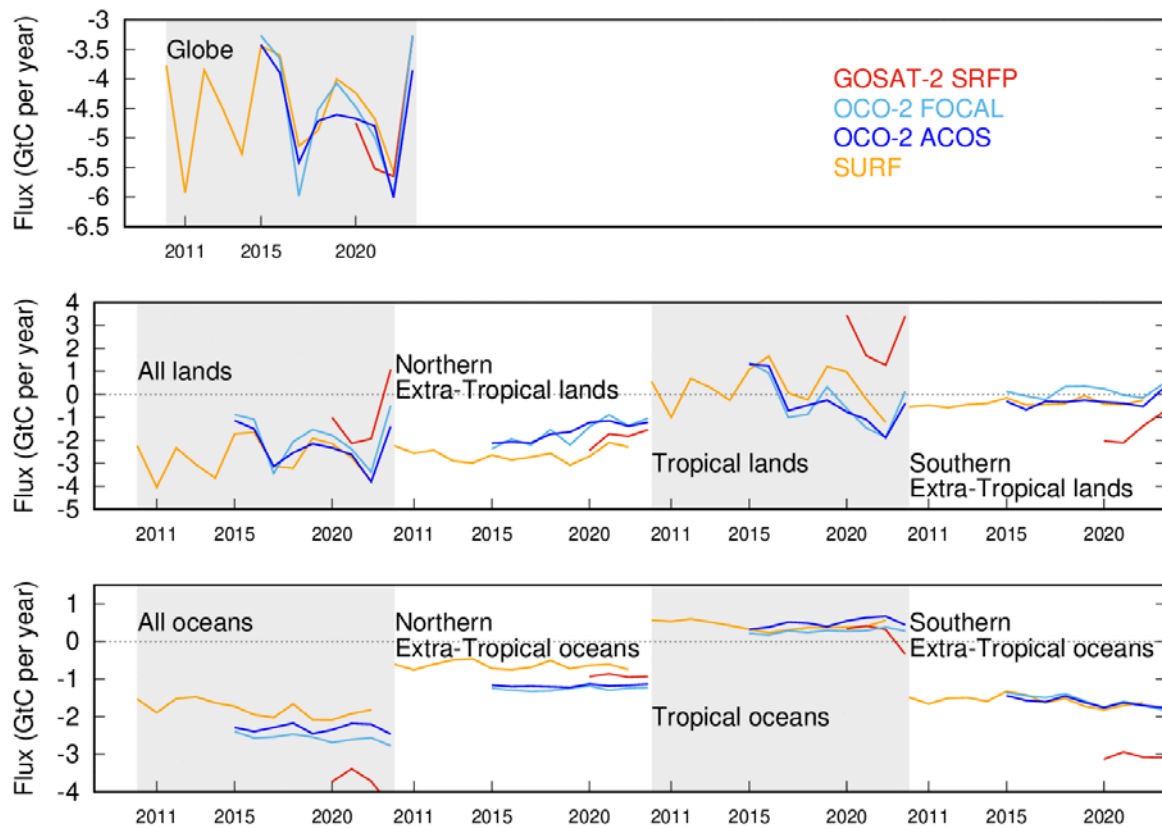


Figure 2. Inferred natural CO<sub>2</sub> annual flux (without fossil fuel emissions) averaged over the globe or over all lands or oceans. In the case of lands and oceans, three broad latitude bands are also defined: northern extra-Tropics (north of 25°N), Tropics (within 25° of the Equator), and southern extra-Tropics (south of 25°S). The blue and orange curves correspond to the CAMS surface-driven (SURF) and OCO-2-driven (ACOS) products. In the sign convention, positive fluxes correspond to a net carbon source into the atmosphere.

## Climate Assessment Report (CAR) for Climate Research Data Package 9 (CRDP#9)

Version 2.1

 of the Essential Climate Variable (ECV)  
Greenhouse Gases (GHG)

6 February 2025

### 3.6. Fit to unassimilated upper-air measurements

Following the approach defined in Chevallier et al. (2019) and applied in GCP's Global Carbon Budget since then (see, e.g., Figure S4 of Friedlingstein et al. 2023), Figure 3 focusses on the dry air mole fraction measurements made by aircraft and Aircore devices in the free troposphere. The free troposphere is simply defined here as the atmospheric layer between 2 and 7 km above sea level. The measurements are here from NOAA's ObsPack Globalview+<sub>v9.1</sub> and ObsPack NRT\_9.3 for the period January 2015 – December 2023. We restrict this study to CO<sub>2</sub>\_OC2\_FOCAL because the other CRDP dataset only covers five full years and appears to be less realistic from the above diagnostics.

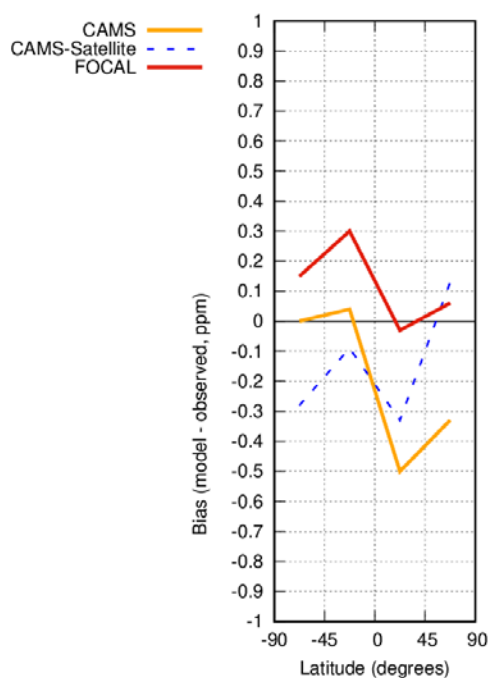


Figure 3. The mean of the model minus observations is shown for four latitude bands and years 2015 – 2023. The three inversions are compared to independent CO<sub>2</sub> measurements made aboard aircraft or Aircore devices over many areas of the world between 2 and 7 km above sea level. Aircraft and Aircore measurements archived in NOAA's ObsPack Globalview+<sub>v9.1</sub> and ObsPack NRT\_9.3 have been used to compute the statistics of the differences in four 45° latitude bins. Land and ocean data are used without distinction, and observation density varies strongly with latitude and time, as seen in the lower panels. Adapted from Friedlingstein et al. (2023).

The model values are strikingly different from the upper-air measurement for none of the three inversions, and none exceeds the symbolic 0.5 ppm bias threshold. Biases are overall comparable to those of the inversions selected by the GCP (Figure S4 of Friedlingstein et al. 2023). In the detail of the measurement programmes (Figure 4), the CO<sub>2</sub>\_OC2\_FOCAL inversion is also comparable to the CAMS inversion driven by NASA's OCO-2 land retrievals, both in terms of bias and in terms of standard deviation of the misfits.

**Climate Assessment Report (CAR)  
for Climate Research Data Package 9 (CRDP#9)**

Version 2.1

of the Essential Climate Variable (ECV)  
Greenhouse Gases (GHG)

6 February 2025

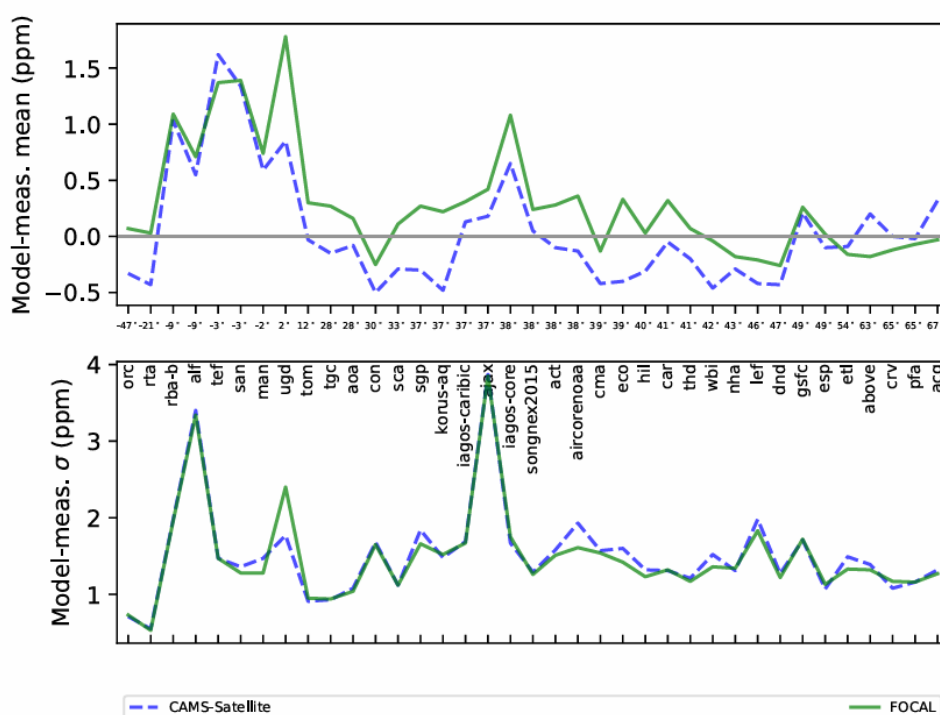


Figure 4. The mean (top) and standard deviation (bottom) of the model minus observations is shown for each measurement programme in the two ObsPack databases in years 2015 – 2023, for the CAMS OCO-2-driven inversion and the CO2\_OC2\_FOCAL inversion. Only statistics including at least 100 measurements made aboard aircraft or Aircore devices between 2 and 7 km above sea level are used. The programmes are ranked by increasing mean latitude (North is on the right), irrespective of their latitudinal coverage (which is large of several tens of degrees for ORC, TOM and CON). These mean latitudes are shown in the middle of the panel. Campaign 'flagg-md' has been excluded as it focused on emissions from an urban center and local power plants.

### 3.7. Conclusions

For the first time in the series of Climate Assessment Reports, a CRDP product yields global inversion results that seem realistic. Within the CAMS/LSCe inversion system, the CO2\_OC2\_FOCAL-driven inversion fits independent upper-air measurements as well as the official CAMS inversions, yields a global distribution of CO<sub>2</sub> sources and sinks comparable to them. Only the inversion posterior growth rate, which differs from the NOAA marine boundary layer estimate by  $0.03 \pm 0.24$  ppm/a over years 2015-2023, is not aligned with the CAMS standard. However, the assimilation of the CO2\_GO2\_SRFp product in the CAMS/LSCe global inversion system still infers a latitudinal distribution of CO<sub>2</sub> surface fluxes that is very different from that obtained by both the assimilation of surface air-sample measurements and the assimilation of NASA's retrievals from OCO-2. We think that it is less credible because it yields a much poorer simulation of the atmospheric growth rate (with a difference to NOAA's estimate of  $-0.02 \pm 0.28$  ppm for 2020-2023).

The consistent results obtained in the CAMS inversions between the surface air-sample measurements and the ACOS retrievals demonstrates that there is no fundamental limitation in

	ESA Climate Change Initiative (CCI+)	Page 20
	<b>Climate Assessment Report (CAR)</b> <b>for Climate Research Data Package 9 (CRDP#9)</b>	Version 2.1
	of the Essential Climate Variable (ECV) Greenhouse Gases (GHG)	6 February 2025

atmospheric inverse modelling (e.g., in the realism of the transport model or in the modelled error statistics) when assimilating satellite XCO<sub>2</sub> retrievals. The ACOS-driven CO<sub>2</sub> surface fluxes have actually been part of the official CAMS data portfolio since year 2019 and several ACOS-driven inversions pass the quality control of GCP’s Global Carbon Budget (Friedlingstein et al. 2023). This potential of satellite XCO<sub>2</sub> retrievals is now also confirmed by the good results obtained with CO2\_OC2\_FOCA in this CRDP release. Interestingly, our test with the CO2\_OC2\_FOCA includes the ocean glint retrievals, while the CAMS product still blacklists NASA’s ones.

For CO2\_GO2\_SRF, we note that so far GOSAT-driven inversions have not reach the quality of OCO-2 driven ones to our best knowledge, and we may meet such a limitation with GOSAT-2 as well, due to the instrument quality joined to its sampling strategy. However, even with this challenge in mind, the simulation of the atmospheric growth rate still seems to be particularly poor.

About computational effort, CO2\_OC2\_FOCA’s distinct advantage compared to ACOS is its representation of multiple scattering effects in the radiative transfer in a form that is not costlier than absorption. In preparation for the Copernicus CO<sub>2</sub> Monitoring Mission that will provide even larger amount of data than OCO-2 (Pinty et al., 2017), the processing of the OCO-2 archive, which is very large by today’s standards, by CO2\_OC2\_FOCA represents an important achievement. In this context and resources permitting, it would be important to document their performance in more detail in order to help prioritize future developments.

## 4. Assessment of satellite-derived XCH<sub>4</sub> data products

### 4.1. Introduction

Global methane inversions based on satellite measurements are well established, going back to the initial SCIAMACHY XCH<sub>4</sub> dataset from 2003, followed by over a decade of soundings from GOSAT. GOSAT data had improved stability and measurement precision, but sparser data coverage. With the launch of Sentinel-5 Precursor (S5P) in October 2017, satellite-based measurements of XCH<sub>4</sub> moved from experimental measurements to an operational product, with vastly increased data density through a smaller footprint (7 km x 5.5 km at nadir) and a continuous wide swath (2600 km). A year later, in October 2018, the Japanese satellite GOSAT-2 was launched, the successor to the successful GOSAT mission.

Here we present an initial user assessment of data products from the 9<sup>th</sup> GHG-CCI+ Climate Research Data Package (CRDP#9, please visit <https://climate.esa.int/en/projects/ghgs/> and click on -> “Data” (for data access information) or -> “Key Documents” (for documentation)).

CRDP#9 consists of the following three CH<sub>4</sub> products (retrieved from two satellite sensors using different retrieval algorithms):

- CH4\_S5P\_WFMD: retrieved from TROPOMI on S5P using the University of Bremen’s WFMD algorithm
- CH4\_GO2\_SRFP: retrieved from GOSAT-2 using SRON’s full physics RemoTeC algorithm
- CH4\_GO2\_SRPR: from GOSAT-2 using SRON’s proxy RemoTeC algorithm, retrieving the ratio of CH<sub>4</sub> to CO<sub>2</sub>

Product ID	Instrument	Algorithm	Data provider	Reference	Period available	Evaluators (sections)
CH4_S5P_WFMD	TROPOMI	WFMD v1.8	IUP, Univ. Bremen	Schneising et al., 2019	11/2017-12/2023	DLR (4.2 – 4.7)
CH4_GO2_SRFP	GOSAT-2	RemoTeC v2.0.3	SRON	Krisna et al., 2022a	02/2019-12/2023	DLR (4.2 – 4.7)
CH4_GO2_SRPR	GOSAT-2	RemoTeC v2.0.3	SRON	Krisna et al., 2022b	02/2019-12/2023	DLR (4.2 – 4.7)
CH4_S5P_SRON	TROPOMI	RemoTeC v2.5.0	SRON	Hu et al., 2016; Lorente et al., 2021	04/2018-12/2023	DLR (4.2 – 4.7)

Table 2: XCH<sub>4</sub> products evaluated in this report. Only the first three are officially members of CRDP#8, but the operational SRON retrievals of S5P measurements is included for context and completeness.

The GOSAT-2 retrievals are now available from February 2019 through the end of 2023, providing almost five full years of data, allowing for a more full assessment of the performance over time.

	ESA Climate Change Initiative (CCI+)	Page 22
	<b>Climate Assessment Report (CAR)</b> for Climate Research Data Package 9 (CRDP#9)	Version 2.1
	of the Essential Climate Variable (ECV) Greenhouse Gases (GHG)	6 February 2025

To enrich the comparison, the operational retrieval of XCH<sub>4</sub> from S5P (Hu et al., 2016, with updates described in Lorente et al., 2021) is also included in the analysis, and is referred to as CH<sub>4</sub>\_S5P\_SRON in the text. The evaluated XCH<sub>4</sub> products are summarized in Table 2.

## 4.2. Preprocessing of satellite retrievals

### 4.2.1. Method

In this section we plot a month's worth of each of the data products to give an impression of the differences in spatial distribution, and illustrate what this difference in data coverage means when aggregated onto the spatial grid of the global transport model used in the inversion.

We then compare the different satellite products with concentration fields resulting from a forward simulation of the TM3 transport model (Heimann and Körner, 2003) using optimized fluxes from an inversion assimilating flask measurements from 76 surface sites covering the full simulation period (2018-2023), using data provided by the ObsPack v6.0 release up to the end of 2022, and the ObsPack NRT v6.2 release for more recent measurements (Schindt et al., 2023 and 2024). The inversion was carried out using the Jena CarboScope variational inversion system (based on Rödenbeck et al., 2003). The transport is carried out at 3.8° latitude by 5° longitude resolution and with 19 vertical levels, and is driven by meteorological fields from the ERA5 reanalysis.

Because the model transport is imperfect, especially with respect to the tropopause height and the gradient of methane within the stratosphere, the comparison to the surface-optimized fields is used to derive a model-specific bias correction. The bias correction is modelled as a 2<sup>nd</sup> order polynomial as a function of latitude and month, following the approach of Bergamaschi et al. (2007) (see Equation 4 from this paper). Because this correction is independent of longitude, the information about local gradients is largely maintained, while ensuring that the model can simultaneously interpret total-column and surface-based measurements of CH<sub>4</sub> in a consistent manner.

When comparing the modelled XCH<sub>4</sub> columns to the XCH<sub>4</sub> measurements, both the prior profile and the averaging kernel are taken into account. Because the spatial resolution of the S5P measurements is so much higher than that of the model fields, we average them to create super-observations for use in the inversion. From CAR8 this has been done in the following manner:

- Count all retrievals with quality flag "good" (or, for CH<sub>4</sub>\_S5P\_SRON, those with qa filter > 0.5) that fall within a model doxel (gridbox per orbit)
- Average the XCH<sub>4</sub> values, weighted by the inverse of measurement precision
- Calculate the mean averaging kernel, averaging per retrieval layer, weighted by the inverse of the measurement precision
- Determine the super-obs measurement precision, as described in Table 3

As described in some detail in CAR#8, the measurement uncertainties reported in CH<sub>4</sub>\_S5P\_SRON are unrealistically low. As such, the decision was made to double the reported measurement

uncertainty. Considering the standard deviation of all XCH<sub>4</sub> measurements within one doxel helps account for the representation error of such highly-resolved measurements in a coarse global model.

TROPOMI retrieval	CH4_S5P_WFMD	CH4_S5P_SRON
The maximum of:	The weighted mean of the reported measurement uncertainty	Double the weighted mean of the reported measurement uncertainty
	The standard deviation of all XCH <sub>4</sub> measurements in the doxel	The standard deviation of all XCH <sub>4</sub> measurements in the doxel

Table 3: Overview of the method for calculating the measurement uncertainty of the aggregated superobs used in the inversion.

#### 4.2.2. Data coverage and creation of super-observations

**TROPOMI:** The spatial coverage of the S5P satellite retrievals are shown for January 2020 in Figure 5. Compared to previous versions of the SRON operational retrieval, the difference in the number of good soundings between the two products is no longer as stark. Nonetheless, the WFMD retrieval continues to have more retrievals that pass the quality filtering, both over land and over the ocean, a pattern which is consistent for the full measurement period. This is particularly notable for some areas, such as mountainous regions (e.g. the Andes and the Himalayas), and at very high latitudes, as the cut-off solar zenith angle is different between the two products (70° for CH<sub>4</sub>\_S5P\_SRON vs. 75° for CH<sub>4</sub>\_S5P\_WFMD).

The mean concentrations are generally very similar, though it can be seen that there are more extremely high values in the SRON product for this particular month (e.g. over central Africa). At first glance the TROPOMI retrievals appear quite similar, at least the structures that are captured are the same.

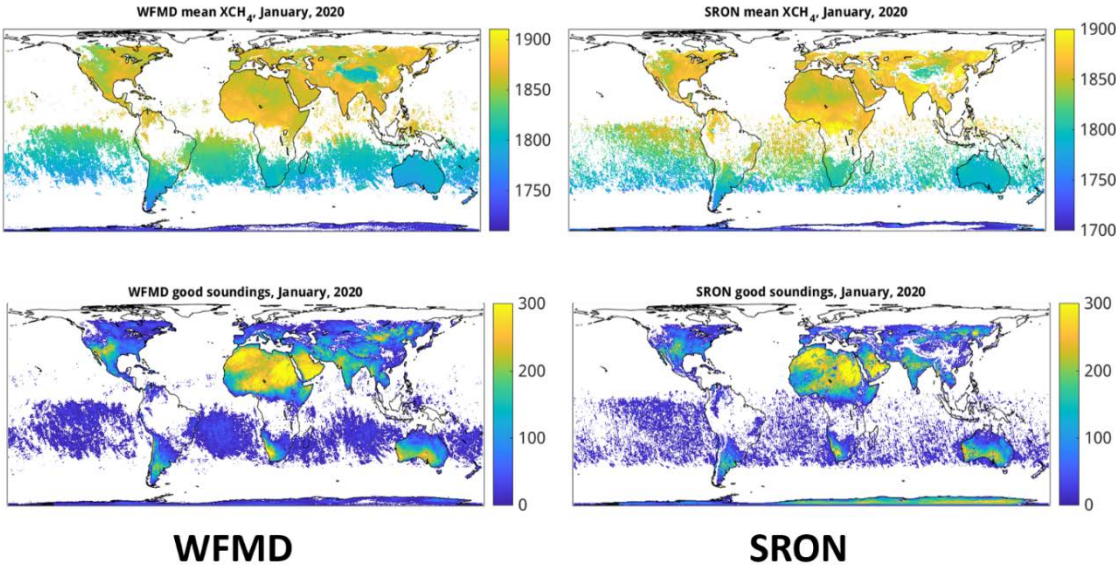


Figure 5: TROPOMI XCH<sub>4</sub> retrievals from the WFMD (left) and SRON (right) products for January, 2020, averaged onto 0.25° x 0.25° bins. The mean XCH<sub>4</sub> values are shown in the top row, and the number of good soundings per bin are shown in the bottom row.

## Climate Assessment Report (CAR) for Climate Research Data Package 9 (CRDP#9)

Version 2.1

of the Essential Climate Variable (ECV)  
Greenhouse Gases (GHG)

6 February 2025

As discussed in Section 4.2.1, these soundings were then aggregated onto the grid resolution of the global transport model to produce super-observations. Figure 6 illustrates that the difference in the number of good soundings largely disappears once aggregated to the coarser model doxels. The next step in creating the superobs is to calculate the uncertainties as described in Table 3.

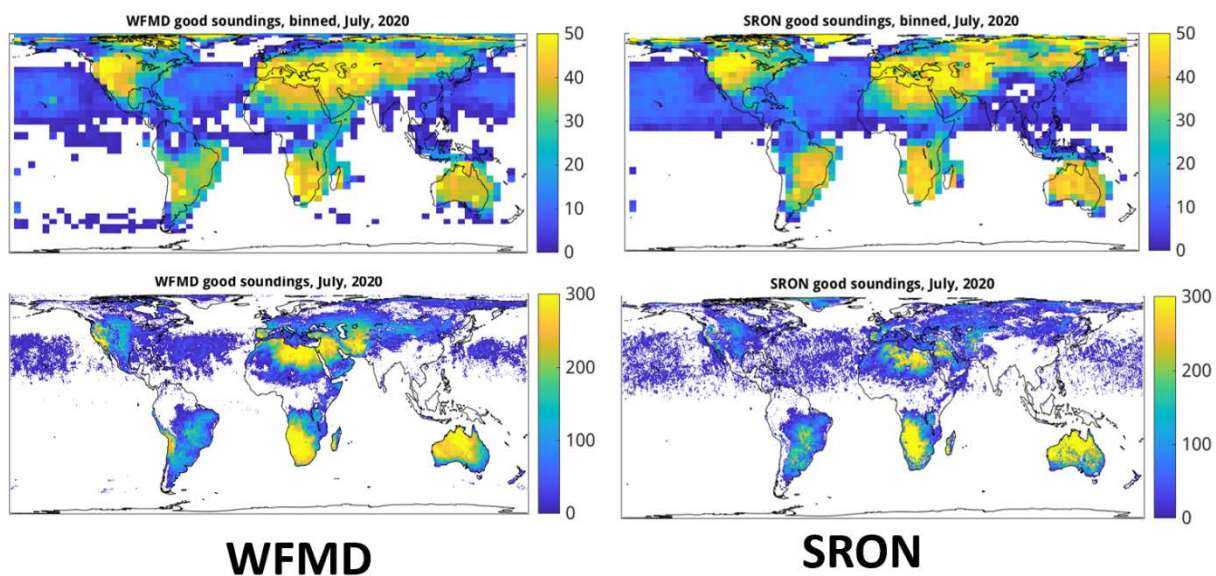


**Figure 6:** Number of good soundings for July, 2020 for WFMD (left) and SRON (right). The number of good superobs for the same month are shown aggregated onto the TM3 grid in the top row, while the number binned at  $0.25^\circ \times 0.25^\circ$  resolution is shown below.

**GOSAT-2:** The data coverage for the proxy and full-physics retrievals for GOSAT-2 (CH<sub>4</sub>\_GO<sub>2</sub>\_SRPR and CH<sub>4</sub>\_GO<sub>2</sub>\_SRFP, respectively) are shown in Figure 7. As expected, the proxy product (CH<sub>4</sub>\_GO<sub>2</sub>\_SRPR) has more measurements and thus, more coverage, than the full-physics retrieval (CH<sub>4</sub>\_GO<sub>2</sub>\_SRFP). Because these data are comparatively sparse, they are assimilated individually, and superobservations are not used. The number of good soundings at model resolution (in Figure 7) is shown only for comparability with the WFMD data coverage shown in Figure 6.

**Bias correction:** As introduced in Section 4.2.1, a 2<sup>nd</sup>-degree polynomial was fit to describe the mismatch between the XCH<sub>4</sub> retrievals and optimized model fields based on surface measurements only.

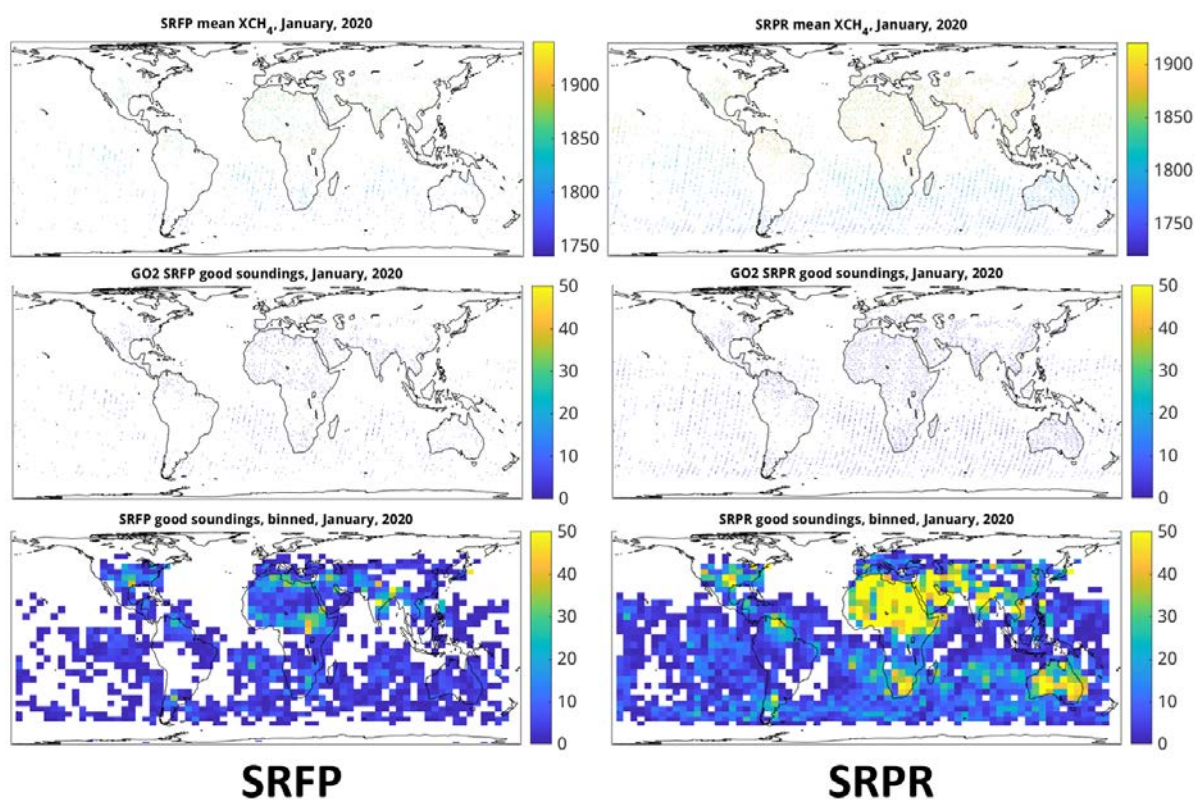


Figure 7: Mean XCH<sub>4</sub> values binned at 0.25° x 0.25° resolution (top row) for January, 2020, for the GOSAT-2 retrieval products CH<sub>4</sub>\_GO2\_SRFP (left) and CH<sub>4</sub>\_GO2\_SRPR (right), with the number of good soundings per bin (middle row). The bottom row shows the number of good soundings over the month when aggregated onto the spatial grid of the global model.

### 4.3. Methane inversion experiments with the Jena CarboScope

After applying the bias corrections to the measurements, aggregated into super-observations, the two TROPOMI XCH<sub>4</sub> retrieval products and the two GOSAT-2 products were assimilated into the Jena CarboScope inversion system to attain optimized fluxes. The satellite data were assimilated alone, without combining them with other observations, in order to focus on the signals inherent to the measurements. From a scientific point of view this may not be the optimal approach: including continuous high-precision surface measurements can have a stabilizing effect on the results. However, it can be difficult to simultaneously assimilate both due to inconsistencies in the information content even after model-specific bias correction. Because the goal of this assessment is to examine the retrieval products on their own merit, the decision was made to not to combined the data streams, but rather keep them separate. The Jena CarboScope system is a variational inversion system, optimizing for the total methane fluxes, based on prior fluxes from bottom-up inventories and process models. The fluxes are optimized on a grid cell level, with category-based correlation lengths in space and time.

	ESA Climate Change Initiative (CCI+)	Page 26
	<b>Climate Assessment Report (CAR)</b> <b>for Climate Research Data Package 9 (CRDP#9)</b>	Version 2.1
	of the Essential Climate Variable (ECV) Greenhouse Gases (GHG)	6 February 2025

The fluxes inferred from these satellite inversions are compared to the inversion over the same time period using the 76 flask sites, as described previously.

#### 4.4. Global mean atmospheric mixing ratio and growth rate

Similar to the approach for CO<sub>2</sub> in Section 3.3, the results from the inversions are compared to global estimates derived directly from the flask measurements. In this case, two estimates are used: NOAA estimates the monthly mean global concentration of methane near the surface based on measurements from its network of marine boundary layer sites (Lan et al., 2022; [https://gml.noaa.gov/ccgg/trends\\_ch4/](https://gml.noaa.gov/ccgg/trends_ch4/)). Similarly, the World Data Centre for Greenhouse Gas Measurements (WDCGG) provides a similar monthly measurement based on near-surface measurements, but includes more continental sites in their estimate, which leads to slightly higher estimates than NOAA's. The WDCGG estimates are reported in the annual WMO Greenhouse Gas Bulletin, and are regularly updated on the WDCGG (World Data Centre for Greenhouse Gases) website. Given the short time period available for the CRDP methane datasets being considered in the CAR, an analysis of monthly concentrations is attractive, even though we would expect this quantity to be less robust than an annual value.

To compare these to the optimized fields resulting from the inversion of the different products, the mean methane mixing ratio for each month is taken, averaged at the second-lowest model level over the whole globe and weighted by the area of the gridbox. The result of this comparison is shown in Figure 8. For reference, the concentrations resulting from the prior flux are included as well.

It is immediately clear that the trend in the prior is negative, whereas all the data-based inversion managed to capture the trend found in the NOAA and WDCGG estimates derived directly from station data. (The anomalies at the very start of 2018 should be ignored, as spin-up effects with sparse data coverage.) The two TROPOMI-based inversions agree quite well with one another, and with the surface-based inversion results. The two GOSAT-2-based inversions agree well with one another, though the absolute difference between the TROPOMI-based and GOSAT-2-based inversions is substantial. Indeed, the GOSAT-2 retrievals are lower even than the NOAA value, which represents the marine background sites. This is unexpected, and suggests a low bias.

In terms of magnitude, the TROPOMI-based inversions are nearly identical to the surface-based inversion. This is a notable improvement from previous versions of the CAR. The GOSAT-based inversions have a very pronounced seasonal cycle, but it does not match well with that derived from the surface-based stations. Furthermore, the trend deduced from the CH<sub>4</sub>\_GO<sub>2</sub>\_SRPR diverges from that of CH<sub>4</sub>\_CO<sub>2</sub>\_SRFP, and indeed that of all the other curves, part way through 2022. In Figure 8 this can be seen with the switching of position between the two curves (purple and magenta): while the global near-surface concentrations from CH<sub>4</sub>\_GO<sub>2</sub>\_SRPR were slightly higher than those of CH<sub>4</sub>\_GO<sub>2</sub>\_SRFP from 2019, they switch positions in mid-2022. When looking at the first derivative of these curves (to get the growth rate, not shown here), it is clear that the CH<sub>4</sub>\_GO<sub>2</sub>\_SRPR result

diverges substantially from all other inversions and growth-rate estimates at this time. This does not appear to be a physically realistic finding.

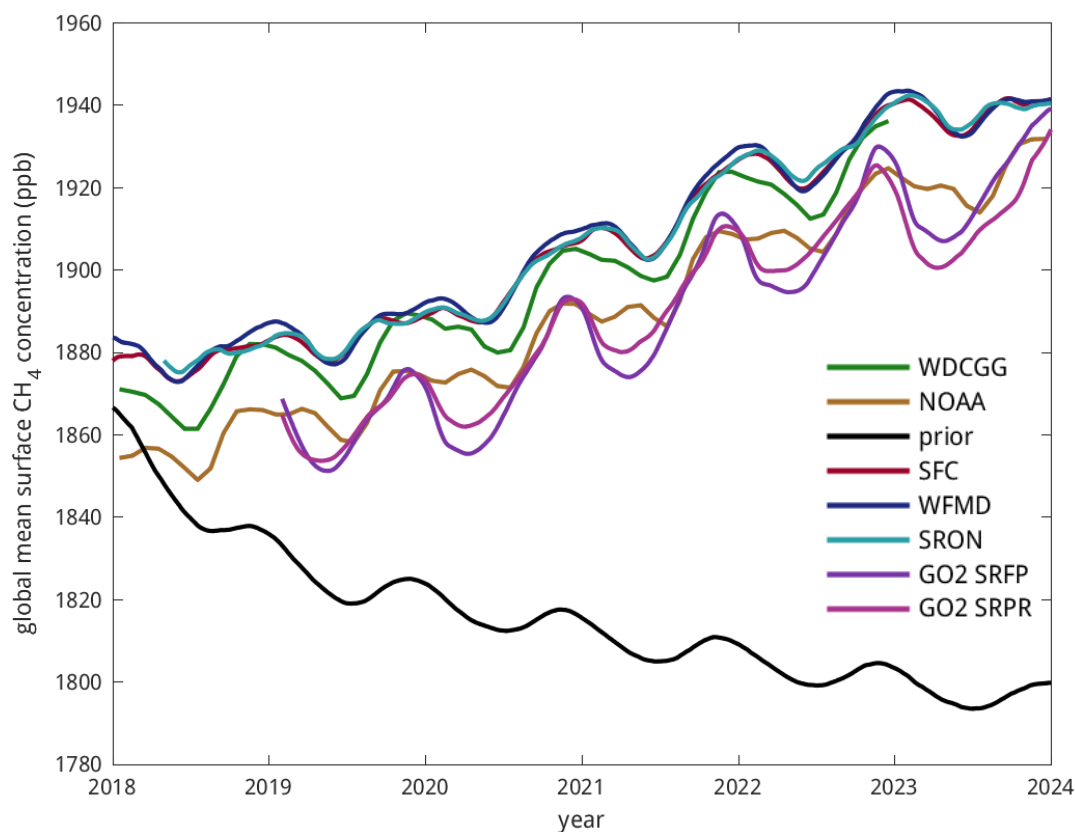


Figure 8: Monthly global mean surface CH<sub>4</sub> mixing ratio at the surface, based directly on in situ measurements (for NOAA in brown and WDCGG in green) or from forward simulations of the prior (in black) or optimized fluxes, based on the surface network (red), CH<sub>4</sub>\_S5P\_WFMD (dark blue), CH<sub>4</sub>\_S5P\_SRON (light blue), CH<sub>4</sub>\_GO2\_SRFP (purple) and CH<sub>4</sub>\_GO2\_SRPR (magenta).

#### 4.5. Comparison of annual flux increments

To assess the spatial patterns inferred from the different inversions, the mean annual increment of the fluxes for 2020 is shown for each of the satellite inversions in Figure 9. The year 2020 was chosen for illustration in order to be able to compare all four satellite-based inversions side by side. Although the magnitudes shifted from year to year, the spatial pattern remained relatively constant.

What is encouraging: all inversions agree on the direction and location of the principal flux increments. These include the general decrease of the prior emissions over parts of China, as well as some increase in emissions in the Southern United States. A further robust pattern is a general increase in emissions from the Tropics. Specifically, all four inversions have larger increases in fluxes

## Climate Assessment Report (CAR) for Climate Research Data Package 9 (CRDP#9)

Version 2.1

of the Essential Climate Variable (ECV)  
Greenhouse Gases (GHG)

6 February 2025

from eastern Africa, which is particularly pronounced for the two GOSAT-2-based inversions, as well as in Indonesia. The pattern over South America is more complex, with both positive and negative anomalies found. Generally, there is a decrease in the prior emissions to the south and west, and a clear increase in emissions closer along the eastern coast of South America. Some reduction in high-latitude emissions in the Northern Hemisphere is also apparent, particularly in the GOSAT-2-based inversions.

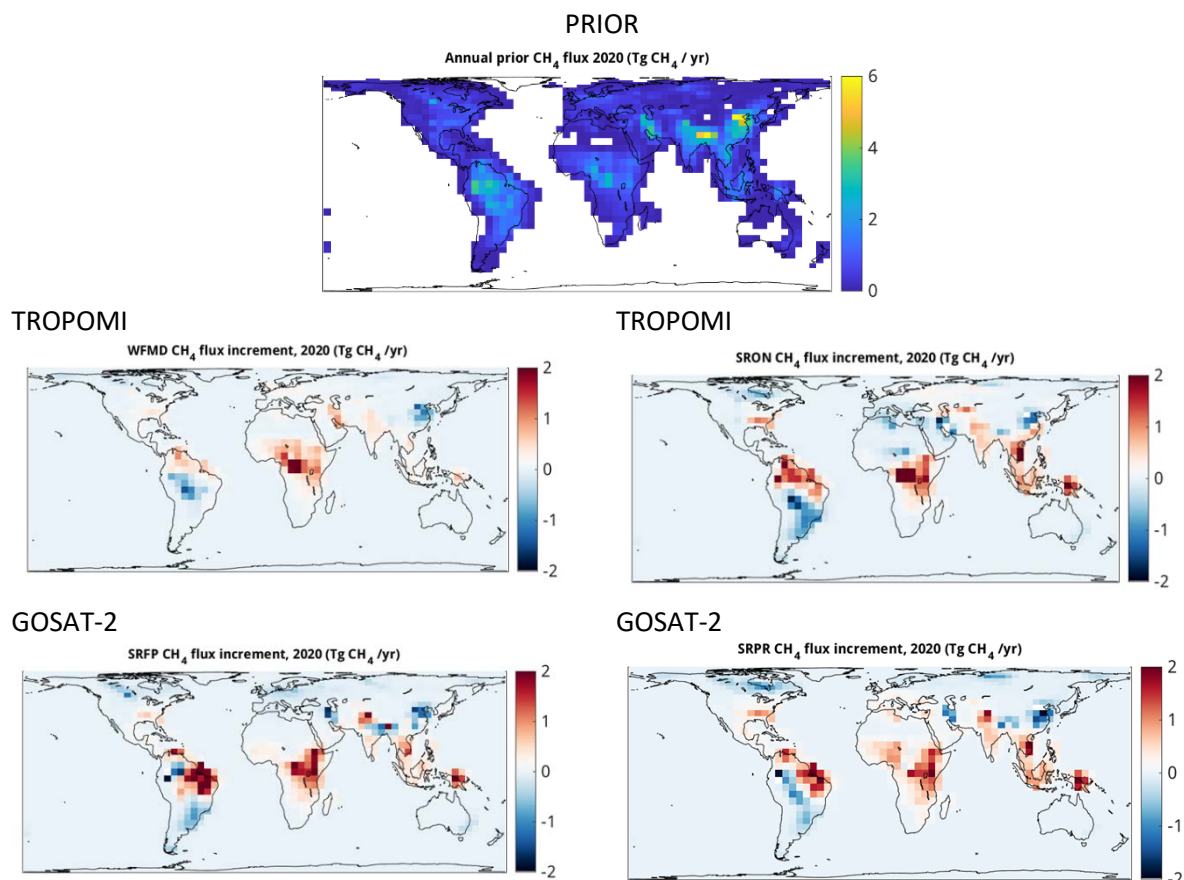


**Figure 9: Annual flux increments for the four satellite-based inversions, along with the prior fluxes (at the top). The two TROPOMI inversions (CH<sub>4</sub>\_S5P\_WFMD, left, and CH<sub>4</sub>\_S5P\_SRON, right) are shown in the middle row, and the two GOSAT-2 inversions (CH<sub>4</sub>\_GO2\_SRFP, left, and CH<sub>4</sub>\_GO2\_SRPR, right) are shown in the bottom row.**

Many of the patterns that are found in these flux increments are consistent with results from previous studies. Specifically:

- Basso et al. (2021) performed regional inversions over the Amazon region based on in situ aircraft-based profiles measurements, and found that the largest methane emissions were from the northeast coast of Brazil, as is seen in the anomaly maps in Figure 9.
- Several studies have shown that global bottom-up emission inventories (in this case, EDGAR 4.3.2) tend to overestimate anthropogenic methane emissions in China (e.g. Chen et al., 2022; Turner et al., 2015; the former based on TROPOMI data, the latter based on GOSAT data). The negative anomalies found in all the inversions confirm this finding.



- The higher East African fluxes and reduced (but still substantial) West African fluxes are consistent with the findings of Lunt et al. (2019), which were based on inversions using GOSAT data.
- The flux anomalies found in North America, with increases in the Central Southern United States and decreases over much of Canada, are consistent with recent findings based on both in-situ and GOSAT-based inversions from Lu et al. (2022).

### 4.6. Evaluation against independent data

As in previous versions of the CAR, the resultant concentrations were compared to independent measurements using TCCON and (limited) aircraft-based measurements. The comparison of the bias and the standard deviation of the residuals from various airborne flight campaigns for flight altitudes up to 6 km is shown in Figure 10.

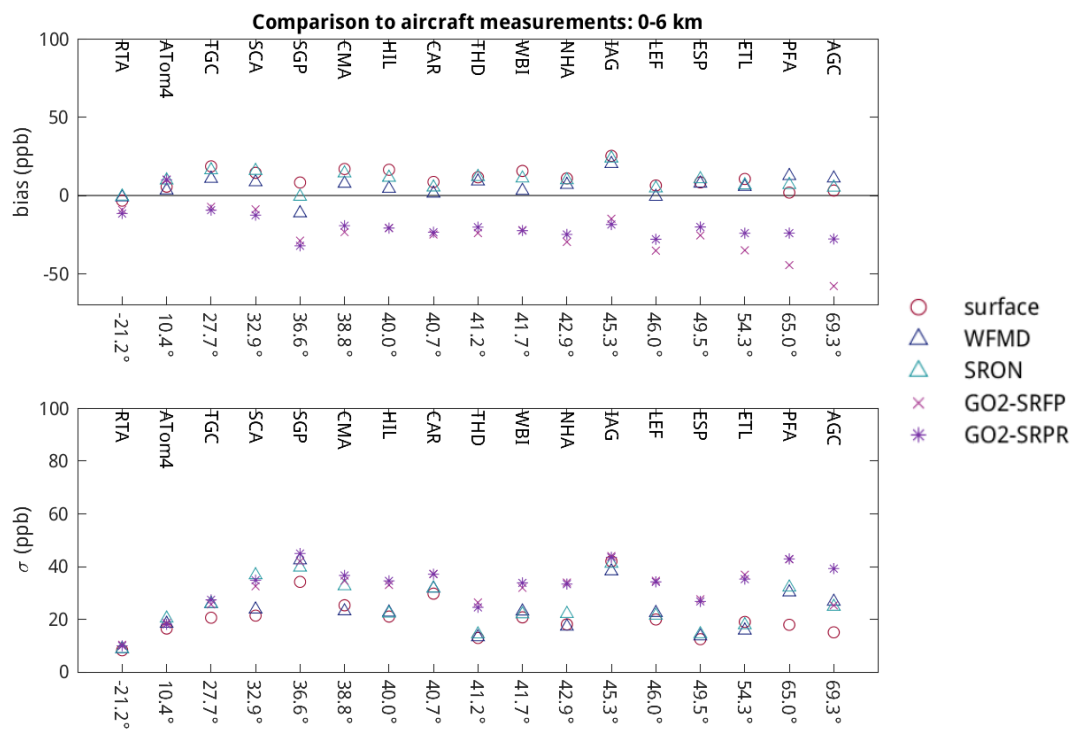


**Figure 10: Comparison of available flight campaign data (from the surface to 6 km) against optimized concentration fields. The top panel shows the mean bias for each dataset, and the bottom panel shows the standard deviation of the residuals, similar to Figure 4 for CO<sub>2</sub>. The average latitude of the record is shown on the x-axis and the code of the data record is on the top of the plot.**

It can be seen that the two TROPOMI-based inversions, as well as the surface-based inversion, have a slight positive bias for most of the locations. The two GOSAT-2-based inversions have a larger negative bias, which is particularly pronounced at high northern latitudes. They also have larger standard deviations in their residuals for almost every location. Note that there is only one flight campaign with an average latitude in the southern hemisphere, in this case all experiments



performed similarly well. It is difficult to choose a “winner” between the CH4\_S5P\_WFMD and CH4\_S5P\_SRON results, as they are quite similar throughout, and perform similarly to the surface-based inversion as well.

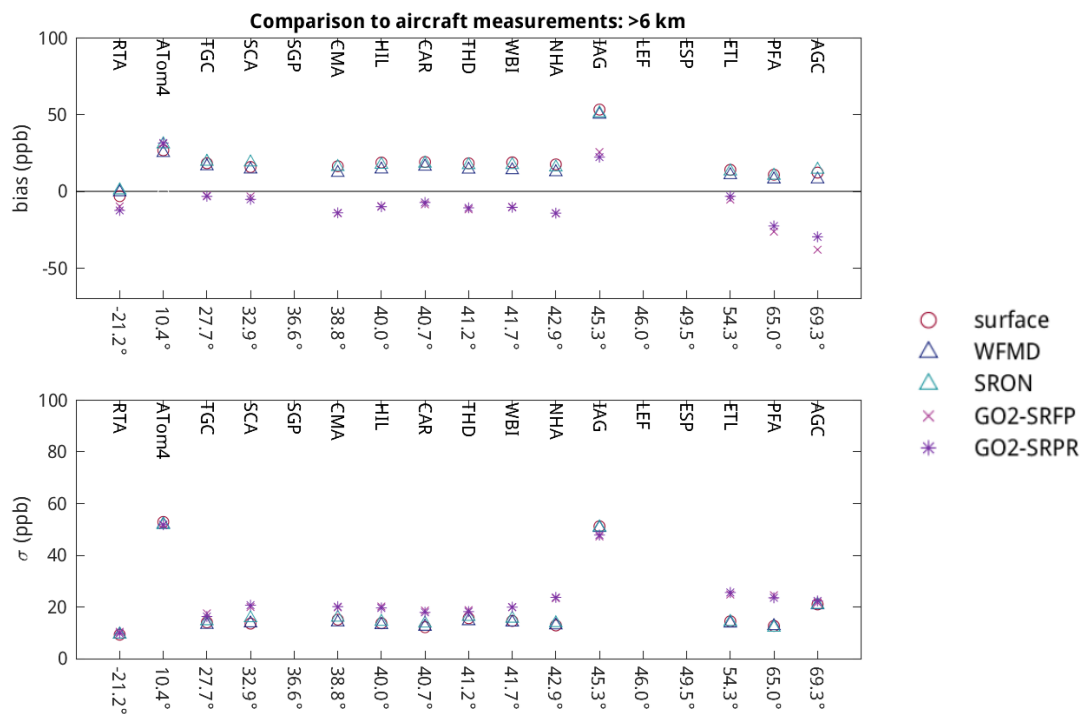


Figure 11: As in Figure 10, but for measurements collected above 6 km. Some sites/campaigns had no data above 6 km, but were included for better comparability.

The same comparison is shown for aircraft-based measurements collected above 6 km altitude in Figure 11. Here the negative bias in the GOSAT-2 simulations is smaller, but still has a latitudinal dependence. Two records, from the ATom-4 flights and the IAGOS data, show very large disagreements. This is due to the fact that these records contain large amounts of data near the tropopause, which is difficult to represent perfectly in a model. When the model is simulating a given altitude as being just below the tropopause whereas the measurement is actually taking place just above the tropopause, a large positive bias is the result.

While the results are again very similar, the CH4\_S5P\_WFMD simulation performs ever so slightly better than the CH4\_S5P\_SRON simulation in most cases.

Finally, the same comparison is carried out against TCCON sites, and can be found in Figure 12. Again, an offset is seen between the GOSAT-2-based inversions and the surface-station-based and TROPOMI-based inversions. This time, however, the latter are biased high compared to the measurements. This illustrates the role of the bias correction, which was not applied in the TCCON analysis. When this is included, the latitudinal dependence largely disappears.

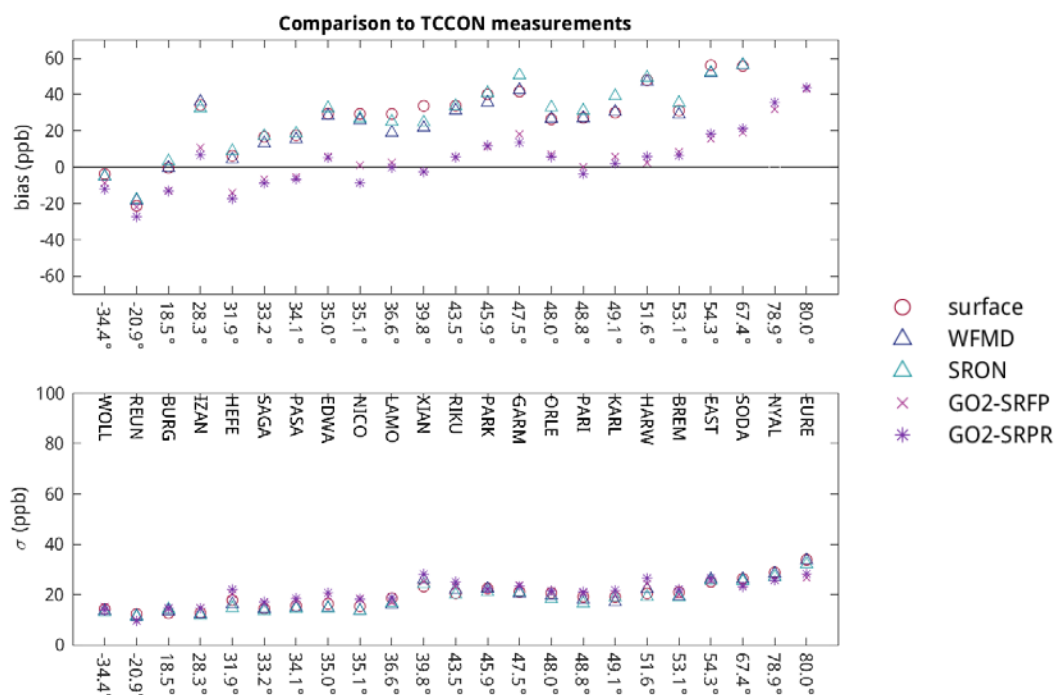


Figure 12: As in Figure 10, but comparing against TCCON total-column measurements.

## 4.7. Conclusions

The fluxes produced by assimilating both the WFMD and the SRON TROPOMI XCH<sub>4</sub> products (CH<sub>4</sub>\_S5P\_WFMD and CH<sub>4</sub>\_S5P\_SRON) into the Jena CarboScope show general structural agreement with each other, and result in very similar near-surface concentrations to those resulting from the assimilation of surface-based measurements alone. This is in contrast to the GOSAT-2-based inversions, which result in a low bias compared to the surface-based and TROPOMI-based inversions, and a very different seasonal cycle. The fact that the surface-based inversions and the TROPOMI-based inversions agree well with each other (see Figure 8) suggests that this is related to a low bias in the GOSAT-2 products. This was confirmed in comparison with independent aircraft-based measurements, which are presented in Section 4.6.

Regardless, the pattern of flux increments is broadly similar when comparing the GOSAT-2-based and TROPOMI-based inversions, showing increases in fluxes in the Tropics, particularly in Indonesia, in Eastern Africa, and large positive anomalies along the northeastern coast in South America. These robust broad patterns are consistent across all the products considered, and are consistent with results from previous studies based on in situ and GOSAT (not GOSAT-2) measurements.

While the results are very similar, the better coverage of the CH<sub>4</sub>\_S5P\_WFMD retrieval, including more retrievals over the oceans, and the slightly better agreement of the optimized concentration

	ESA Climate Change Initiative (CCI+)	Page 32
	<b>Climate Assessment Report (CAR)</b> <b>for Climate Research Data Package 9 (CRDP#9)</b>	Version 2.1
	of the Essential Climate Variable (ECV) Greenhouse Gases (GHG)	6 February 2025

fields with independent measurements makes it the most attractive product for analysis. Though not particularly important when considered in the context of global inversions, v1.8 of CH4\_S5P\_WFMD has also successfully implemented a destriping algorithm, making it more convenient for some regional applications. It also reports realistic measurement uncertainties, unlike the unrealistically low reported uncertainties of CH4\_S5P\_SRON, which need to be inflated by the user to avoid overfitting.

Despite the general agreement that is seen in concentration space, the temporal and spatial variability of the fluxes that arise from the assimilation of TROPOMI XCH<sub>4</sub> are still quite variable in both space and time, leading to unrealistically large seasonal cycles in boreal regions, for example. (This may be related to snowcover effects in the spring, the evidence is inconclusive.) The experimental setup exacerbates this problem: because the XCH<sub>4</sub> products were assimilated alone, there was no stabilizing influence from simultaneously assimilated surface measurements. Because the spatial coverage of the measurements has such a strong seasonal cycle, small systematic errors, especially at high latitudes, can induce unrealistic fluxes. Here the recommendation is rather on the user side: simultaneously assimilating surface-based and satellite data can mitigate these effects.

Despite these concerns, the amount of detailed information about local methane gradients in the TROPOMI retrieval products is extraordinary, and the products have already been used extensively to analyze point sources and local-scale gradients. They are also able to well reproduce global mean mixing ratios over the six years considered in this report. Nonetheless, for their application in global inversion modelling to analyse regional scale fluxes over seasonal and interannual scales, care needs to be taken to ensure that (perhaps small) systematic errors do not bias the resultant fluxes.

	ESA Climate Change Initiative (CCI+)	Page 33
	<b>Climate Assessment Report (CAR)</b> <b>for Climate Research Data Package 9 (CRDP#9)</b>	Version 2.1
	of the Essential Climate Variable (ECV) Greenhouse Gases (GHG)	6 February 2025

## Acknowledgements

F. Chevallier thanks M. Reuter and M. Buchwitz for constructive discussions about the use and the evaluation of these products. He is very grateful to the many people involved in the air-sample measurements and in the archiving of these data. Some of the computations have been performed using HPC resources from CCRT under the allocation A0090102201 made by GENCI (Grand Equipement National de Calcul Intensif). The OCO-2 ACOS data have been obtained from <http://co2.jpl.nasa.gov>. They were produced by the OCO-2 project at the Jet Propulsion Laboratory, California Institute of Technology. CAMS data are publicly available from <http://atmosphere.copernicus.eu/>.

J. Marshall acknowledges the use of computing resources of the Deutsches Klimarechenzentrum (DKRZ) granted by its Scientific Steering Committee (WLA) under project ID bd1231.

	ESA Climate Change Initiative (CCI+)	Page 34
	<b>Climate Assessment Report (CAR)</b> <b>for Climate Research Data Package 9 (CRDP#9)</b>	Version 2.1
	of the Essential Climate Variable (ECV) Greenhouse Gases (GHG)	6 February 2025

## References

### Note:

- **Links to pdf versions of all GHG-CCI+ CRDP documents are available on the GHG-CCI+ key documents website: <https://climate.esa.int/en/projects/ghgs/key-documents/>**
- **Links to pdf versions of all GHG-CCI+ publications are available on the GHG-CCI+ publications website: <https://climate.esa.int/en/projects/ghgs/publications/>**

Alexe, M., P. Bergamaschi, A. Segers, et al., Inverse modeling of CH<sub>4</sub> emissions for 2010–2011 using different satellite retrieval products from GOSAT and SCIAMACHY, *Atmos. Chem. Phys.*, 15, 113–133, doi:10.5194/acp-15-113-2015, 2015.

Balagus, N., Jacob, D. J., Lorente, A., Maasackers, J. D., Parker, R. J., Boesch, H., Chen, Z., Kelp, M. M., Nesser, H., and Varon, D. J.: A blended TROPOMI+GOSAT satellite data product for atmospheric methane using machine learning to correct retrieval biases, *Atmos. Meas. Tech.*, 16, 3787–3807, <https://doi.org/10.5194/amt-16-3787-2023>, 2023.

Basso, L.S., Marani, L., Gatti, L.V. et al. Amazon methane budget derived from multi-year airborne observations highlights regional variations in emissions. *Commun Earth Environ* 2, 246, <https://doi.org/10.1038/s43247-021-00314-4>, 2021.

Bastos, A., Running, S.W., Gouveia, C. and Trigo, R.M: The global NPP dependence on ENSO: La-Nina and the extraordinary year of 2011. *J. Geophys. Res.* 118, 1247–1255, 2013

Basu, S., Guerlet, S., Butz, A., et al., Global CO<sub>2</sub> fluxes estimated from GOSAT retrievals of total column CO<sub>2</sub>, *Atmos. Chem. Phys.*, 13, 8695–8717, 2013.

Basu, S., Krol, M., Butz, A., et al., The seasonal variation of the CO<sub>2</sub> flux over Tropical Asia estimated from GOSAT, CONTRAIL and IASI, *Geophys. Res. Lett.*, doi: 10.1002/2013GL059105, 2014.

Bergamaschi, P., C. Frankenberg, J. F. Meirink, M. Krol, M. G. Villani, S. Houweling, F. Dentener, E. J. Dlugokencky, J. B. Miller, L. V. Gatti, A. Engel, and I. Levin: Inverse modeling of global and regional CH<sub>4</sub> emissions using SCIAMACHY satellite retrievals, *J. Geophys. Res.*, 114, doi:10.1029/2009JD012287, 2009.

Bergamaschi, P., et al.: Inverse modeling of European CH<sub>4</sub> emissions 2001–2006, *J. Geophys. Res.*, 115(D22309), doi:10.1029/2010JD014180, 2010.

Bergamaschi, P., S. Houweling, A. Segers, M. Krol, C. Frankenberg, R. A. Scheepmaker, E. Dlugokencky, S. Wofsy, E. Kort, C. Sweeney, T. Schuck, C. Brenninkmeijer, H. Chen, V. Beck and C. Gerbig, Atmospheric CH<sub>4</sub> in the first decade of the 21st century: Inverse modeling analysis using SCIAMACHY satellite retrievals and NOAA surface measurements, *J. Geophys. Res.*, 118, doi:10.1002/jgrd.50480, 2013.

	ESA Climate Change Initiative (CCI+)	Page 35
	<b>Climate Assessment Report (CAR) for Climate Research Data Package 9 (CRDP#9)</b>	Version 2.1
	of the Essential Climate Variable (ECV) Greenhouse Gases (GHG)	6 February 2025

Bloom, A. A., Palmer, P. I., Fraser, A., and Reay, D. S.: Seasonal variability of tropical wetland CH<sub>4</sub> emissions: the role of the methanogen-available carbon pool, *Biogeosciences*, 9, 2821–2830, doi:10.5194/bg-9-2821-2012, 2012

Boden, T. A., Marland, G., and Andres, R. J.: Global, regional, and national fossil-fuel CO<sub>2</sub> emissions. Carbon Dioxide Information Analysis Center, Oak Ridge National Laboratory, U.S. Department of Energy, Oak Ridge, Tenn., U.S.A., Doi:10.3334/CDIAC/00001\_V2013, 2013

Buchwitz, M., M. Reuter, O. Schneising, et al., The Greenhouse Gas Climate Change Initiative (GHG-CCI): comparison and quality assessment of near-surface-sensitive satellite-derived CO<sub>2</sub> and CH<sub>4</sub> global data sets, *Remote Sensing of Environment*, 162, 344–362, doi:10.1016/j.rse.2013.04.024, 2015.

Buchwitz, M., M. Reuter, O. Schneising, W. Hewson, R.G. Detmers, H. Boesch, O.P. Hasekamp, I. Aben, H. Bovensmann, J.P. Burrows, A. Butz, F. Chevallier, B. Dils, C. Frankenberg, J. Heymann, G. Lichtenberg, M. De Mazière, J. Notholt, R. Parker, T. Warneke, C. Zehner, D.W.T. Griffith, N.M. Deutscher, A. Kuze, H. Suto, D. Wunch, 2017: Global satellite observations of column-averaged carbon dioxide and methane: The GHG-CCI XCO<sub>2</sub> and XCH<sub>4</sub> CRDP3 data set, *Remote Sensing of Environment*, 203, 276-295, [doi:dx.doi.org/10.1016/j.rse.2016.12.027](https://doi.org/10.1016/j.rse.2016.12.027).

Buchwitz, M., Dils, B., Reuter, M., Schneising, O., Hilker, M., Preval, S., Boesch, H., Borsdoff, T., Landgraf, J., Krisna, T.C., Product Validation and Intercomparison Report (PVIR) for the Essential Climate Variable (ECV) Greenhouse Gases (GHG): XCO<sub>2</sub> and/or XCH<sub>4</sub> from OCO-2, TanSat, Sentinel-5-Precursor and GOSAT-2, v3.0, 16 February 2022, 2022.

Butz, A., Guerlet, S., Hasekamp, O., et al., Toward accurate CO<sub>2</sub> and CH<sub>4</sub> observations from GOSAT, *Geophys. Res. Lett.*, doi:10.1029/2011GL047888, 2011.

Byrne, B., Baker, D. F., Basu, S., et al.: National CO<sub>2</sub> budgets (2015–2020) inferred from atmospheric CO<sub>2</sub> observations in support of the global stocktake, *Earth Syst. Sci. Data*, 15, 963–1004, <https://doi.org/10.5194/essd-15-963-2023>, 2023.

Canadell, J. G., Ciais, P., Dhakal, S., et al., Interactions of the carbon cycle, human activity, and the climate system: a research portfolio, *Curr. Opin. Environ. Sustainabil.*, 2, 301–311, 2010.

Chatterjee, A., Gierach, M. M., Sutton, A. J. et al., Influence of El Niño on atmospheric CO<sub>2</sub> over the tropical Pacific Ocean: Findings from NASA's OCO-2 mission. *Science* 358, eaam5776, doi:10.1126/science.aam5776, 2017.

Chen, Z., Jacob, D. J., Nesser, H., Sulprizio, M. P., Lorente, A., Varon, D. J., Lu, X., Shen, L., Qu, Z., Penn, E., and Yu, X.: Methane emissions from China: a high-resolution inversion of TROPOMI satellite observations, *Atmos. Chem. Phys.*, 22, 10809–10826, <https://doi.org/10.5194/acp-22-10809-2022>, 2022.

	ESA Climate Change Initiative (CCI+)	Page 36
	<b>Climate Assessment Report (CAR)</b> for Climate Research Data Package 9 (CRDP#9)	Version 2.1
	of the Essential Climate Variable (ECV) Greenhouse Gases (GHG)	6 February 2025

Chevallier, F., et al.: Inferring CO<sub>2</sub> sources and sinks from satellite observations: method and application to TOVS data. *J. Geophys. Res.*, 110, D24309, 2005.

Chevallier, F.: Impact of correlated observation errors on inverted CO<sub>2</sub> surface fluxes from OCO measurements, *Geophys. Res. Lett.*, 34, L24804, doi:10.1029/2007GL030463, 2007.

Chevallier, F., Maksyutov, S., Bousquet, P., Bréon, F.-M., Saito, R., Yoshida, Y., and Yokota, T.: On the accuracy of the CO<sub>2</sub> surface fluxes to be estimated from the GOSAT observations. *Geophys. Res. Lett.*, 36, L19807, doi:10.1029/2009GL040108, 2009.

Chevallier, F., et al.: CO<sub>2</sub> surface fluxes at grid point scale estimated from a global 21-year reanalysis of atmospheric measurements. *J. Geophys. Res.*, 115, D21307, doi:10.1029/2010JD013887, 2010a.

Chevallier, F., Feng, L., Boesch, H., Palmer, P., and Rayner, P.: On the impact of transport model errors for the estimation of CO<sub>2</sub> surface fluxes from GOSAT observations. *Geophys. Res. Lett.*, 37, L21803, doi:10.1029/2010GL044652, 2010b.

Chevallier, F., Deutscher, N. M., Conway, T. J., Ciais, P., Ciattaglia, L., Dohe, S., Frohlich, M., Gomez-Pelaez, A. J., Griffith, D., Hase, F., Haszpra, L., Krummel, P., Kyro, E., Labuschagne, C., Langenfelds, R., Machida, T., Maignan, F., Matsueda, H., Morino, I., Notholt, J., Ramonet, M., Sawa, Y., Schmidt, M., Sherlock, V., Steele, P., Strong, K., Sussmann, R., Wennberg, P., Wofsy, S., Worthy, D., Wunch, D., and Zimnoch, M.: Global CO<sub>2</sub> fluxes inferred from surface air-sample measurements and from TCCON retrievals of the CO<sub>2</sub> total column, *Geophys. Res. Lett.*, 38, L24810, doi:10.1029/2011GL049899, 2011

Chevallier, F., Bergamaschi, P., Kaminiski, T., Scholze, M., Climate Assessment Report (CAR) for the GHG-CCI project of ESA's Climate Change Initiative, version 1.1 (CARv1.1), 18. Nov. 2013, 2013.

Chevallier, F., and O'Dell, C. W., Error statistics of Bayesian CO<sub>2</sub> flux inversion schemes as seen from GOSAT, *Geophys. Res. Lett.*, doi: 10.1002/grl.50228, 2013.

Chevallier, F., Palmer, P.I., Feng, L., Boesch, H., O'Dell, C.W., Bousquet, P., Towards robust and consistent regional CO<sub>2</sub> flux estimates from in situ and space-borne measurements of atmospheric CO<sub>2</sub>, *Geophys. Res. Lett.*, 41, 1065-1070, DOI: 10.1002/2013GL058772, 2014a.

Chevallier, F., Buchwitz, M., Bergamaschi, et al., User Requirements Document for the GHG-CCI project of ESA's Climate Change Initiative, version 2 (URDv2), 28. August 2014, 2014b.

Chevallier, F.: On the statistical optimality of CO<sub>2</sub> atmospheric inversions assimilating CO<sub>2</sub> column retrievals, *Atmos. Chem. Phys.*, 15, 11133–11145, <https://doi.org/10.5194/acp-15-11133-2015>, 2015.

Chevallier, F., P. Bergamaschi, D. Brunner, S. Gonzi, S. Houweling, T. Kaminski, G. Kuhlmann, T. T. van Leeuwen, J. Marshall, P. I. Palmer, and M. Scholze, Climate Assessment Report for the GHG-CCI project of ESA's Climate Change Initiative, pp. 87, version 2, 22 April 2015, 2015.

	ESA Climate Change Initiative (CCI+)	Page 37
	<b>Climate Assessment Report (CAR)</b> for Climate Research Data Package 9 (CRDP#9)	Version 2.1
	of the Essential Climate Variable (ECV) Greenhouse Gases (GHG)	6 February 2025

Chevallier, F., M. Alexe, P. Bergamaschi, D. Brunner, L. Feng, S. Houweling, T. Kaminski, W. Knorr, T. T. van Leeuwen, J. Marshall, P. I. Palmer, M. Scholze, A.-M. Sundström and M. Voßbeck, Climate Assessment Report for the GHG-CCI project of ESA's Climate Change Initiative, pp. 94, version 3, 3 May 2016, 2016.

Chevallier, F., P. Bergamaschi, D. Brunner, L. Feng, S. Houweling, T. Kaminski, W. Knorr, J. Marshall, P. I. Palmer, S. Pandey, M. Reuter, M. Scholze, and M. Voßbeck, Climate Assessment Report for the GHG-CCI project of ESA's Climate Change Initiative, pp. 96, version 4,, 27 March 2017, 2017.

Chevallier, F., Remaud, M., O'Dell, C. W., Baker, D., Peylin, P., and Cozic, A.: Objective evaluation of surface- and satellite-driven carbon dioxide atmospheric inversions, *Atmos. Chem. Phys.*, 19, 14233–14251, <https://doi.org/10.5194/acp-19-14233-2019>, 2019.

Chevallier, F., Climate Assessment Report for the GHG-CCI+ project of ESA's Climate Change Initiative, pp. 36, version 1.2, 20 March 2020, 2020.

Chevallier, F. and Marshall, J., Climate Assessment Report for the GHG-CCI+ project of ESA's Climate Change Initiative, pp. 59, version 2.0, 9 March 2021, 2021.

Chevallier, F. and Marshall, J., Climate Assessment Report for Climate Research Data Package No. 8 (CRDP#8) of ESA's Climate Change Initiative project GHG-CCI+, version 1.0, 8 Feb. 2024, 2024.

Chevallier, F., Evaluation and Quality Control document for observation-based CO<sub>2</sub> flux estimates for the period 1979 – 2022, v22r1. CAMS deliverable CAMS255\_2021SC1\_D55.1.4.2-2023\_202308. <http://atmosphere.copernicus.eu/>, 2023.

Chevallier, F., Evaluation and Quality Control document for the observation-based flux estimates for CO<sub>2</sub> based on OCO-2 satellite observations during 2024 – Release 2. CAMS deliverable CAMS255\_bis\_2023SC1\_D1.2.2-2024R2\_202407. <http://atmosphere.copernicus.eu/>, 2024.

Chevallier, F. and Marshall, J., Climate Assessment Report for Climate Research Data Package No. 7 (CRDP#7) of ESA's Climate Change Initiative project GHG-CCI+, version 1.1, 20 March 2023, 2023.

Chevallier, F., Lloret, Z., Cozic, A., Takache, S., & Remaud, M. (2023). Toward high-resolution global atmospheric inverse modelling using graphics accelerators. *Geophysical Research Letters*, 50, e2022GL102135. <https://doi.org/10.1029/2022GL102135>

Cogan, A. J., Boesch, H., Parker, R. J., et al., Atmospheric carbon dioxide retrieved from the Greenhouse gases Observing SATellite (GOSAT): Comparison with ground-based TCCON observations and GEOS-Chem model calculations, *J. Geophys. Res.*, 117, D21301, doi:10.1029/2012JD018087, 2012.

Conway, T. J., Tans, P. P., Waterman, L. S., Thoning, K. W., Kitzis, D. R., Masarie, K. A. and Zhang, N.: Evidence for interannual variability of the carbon cycle from the National Oceanic and Atmospheric Administration/Climate Monitoring and Diagnostics Laboratory Global Air Sampling Network, *J. Geophys. Res.*, 99(D11), 22,831–22,855, doi:10.1029/94JD01951, 1994

**Climate Assessment Report (CAR)  
for Climate Research Data Package 9 (CRDP#9)**

Version 2.1

of the Essential Climate Variable (ECV)  
Greenhouse Gases (GHG)

6 February 2025

Cramer, W., Kicklighter, D. W., Bondeau, A., Iii, B. M., Churkina, G., Nemry, B., Ruimy, A., Schloss, A. L. and Intercomparison, ThE. P. OF. ThE. P. NpP. M., Comparing global models of terrestrial net primary productivity (NPP): overview and key results. *Global Change Biology*, 5: 1–15. doi:10.1046/j.1365-2486.1999.00009.x, 1999.

Cressot, C., F. Chevallier, P. Bousquet, et al., On the consistency between global and regional methane emissions inferred from SCIAMACHY, TANSO-FTS, IASI and surface measurements, *Atmos. Chem. Phys.*, 14, 577-592, 2014.

Cressot, C., Pison, I., Rayner, P. J., Bousquet, P., Fortems-Cheiney, A., and Chevallier, F.: Can we detect regional methane anomalies? A comparison between three observing systems, *Atmos. Chem. Phys.*, 16, 9089-9108, doi:10.5194/acp-16-9089-2016, 2016.

Crevoisier, C., Sweeney, C., Gloor, M., Sarmiento, J. L., and Tans, P. P.: Regional U.S. carbon sinks from three-dimensional atmospheric CO<sub>2</sub> sampling, *Proc. Natl. Acad. Sci.* (2010), 107: 18348-18353, 2010.

Crowell, S., Baker, D., Schuh, A., Basu, S., Jacobson, A. R., Chevallier, F., Liu, J., Deng, F., Feng, L., McKain, K., Chatterjee, A., Miller, J. B., Stephens, B. B., Eldering, A., Crisp, D., Schimel, D., Nassar, R., O'Dell, C. W., Oda, T., Sweeney, C., Palmer, P. I., and Jones, D. B. A.: The 2015–2016 carbon cycle as seen from OCO-2 and the global in situ network, *Atmos. Chem. Phys.*, 19, 9797–9831, <https://doi.org/10.5194/acp-19-9797-2019>, 2019.

Dee, D. P., et al., The ERA-Interim reanalysis: configuration and performance of the data assimilation system, *Q. J. R. Meteorol. Soc.*, 137, 553–597, 2011.

Desroziers G., Berre, L., Chapnik, B., and Poli, P.: Diagnosis of observation, background and analysis error statistics in observation space. *Q. J. Roy. Meteor. Soc.*, 131, 3385-3396, 2005.

Detmers, R., Hasekamp, O., Aben, I., Houweling, S., van Leeuwen, T.T., Butz, A., Landgraf, J., Kohler, P., Guanter, L., and Poulter, B.: Anomalous carbon uptake in Australia as seen by GOSAT. *Geophysical Research Letters*, 42(19), 2015

Dlugokencky, E. J., L. P. Steele, P. M. Lang, and K. A. Masarie, The growth rate and distribution of atmospheric methane, *J. Geophys. Res.*, 99, 17021–17043. 1994.

Dlugokencky, E. J., S. Houweling, L. Bruhwiler, K. A. Masarie, P.M. Lang, J. B. Miller, and P. P. Tans, Atmospheric methane levels off: Temporary pause or a new steady-state? *Geophys. Res. Lett.*, 30(19), 1992, doi:10.1029/2003GL018126, 2003.

Dlugokencky, E. J., Bruhwiler, L., White, J. W. C., et al., Observational constraints on recent increases in the atmospheric CH<sub>4</sub> burden, *Geophys. Res. Lett.*, 36, L18803, doi:10.1029/2009GL039780, 2009.

	ESA Climate Change Initiative (CCI+)	Page 39
	<b>Climate Assessment Report (CAR)</b> for Climate Research Data Package 9 (CRDP#9)	Version 2.1
	of the Essential Climate Variable (ECV) Greenhouse Gases (GHG)	6 February 2025

Dlugokencky, E., P. Lang, J. Mund, A. Crostwell, M. Crostwell, and K. Thoning, Atmospheric carbon dioxide dry air mole fractions from the NOAA ESRL carbon cycle cooperative global air sampling network, 1968-2015, 2016.

Dubovik, O. and King, M. D.: A flexible inversion algorithm for retrieval of aerosol optical properties from Sun and sky radiance measurements, *J. Geophys. Res.*, 105, 20673–20696, 2000.

Enting, I. G.: Inverse Problems in Atmospheric Constituent Transport. Cambridge University Press, 2002.

ESA: A-SCOPE - Advanced Space Carbon and Climate Observation of Planet Earth, Technical Report SP-1313/1, European Space Agency, Noordwijk, The Netherlands. 2008

Feng, L., Palmer, P. I., Bösch, H., and Dance, S.: Estimating surface CO<sub>2</sub> fluxes from space-borne CO<sub>2</sub> dry air mole fraction observations using an ensemble Kalman Filter, *Atmos. Chem. Phys.*, 9, 2619–2633, doi:10.5194/acp-9-2619-2009, 2009.

Feng, L., P. I. Palmer, R. J. Parker, et al., Estimates of European uptake of CO<sub>2</sub> inferred from GOSAT X<sub>CO2</sub> retrievals: sensitivity to measurement bias inside and outside Europe, *Atmos. Chem. Phys.*, 16, 1289-1302, doi:10.5194/acp-16-1289-2016, 2016a.

Feng, L., Palmer, P. I., Bösch, H., Parker, R. J., Webb, A. J., Correia, C. S. C., Deutscher, N. M., Domingues, L. G., Feist, D. G., Gatti, L. V., Gloor, E., Hase, F., Kivi, R., Liu, Y., Miller, J. B., Morino, I., Sussmann, R., Strong, K., Uchino, O., Wang, J., and Zahn, A.: Consistent regional fluxes of CH<sub>4</sub> and CO<sub>2</sub> inferred from GOSAT proxy XCH<sub>4</sub>:XCO<sub>2</sub> retrievals, 2010–2014, *Atmos. Chem. Phys. Discuss.*, doi:10.5194/acp-2016-868, in review, 2016b. Frankenberg, C., Aben, I., Bergamaschi, P., et al., Global column-averaged methane mixing ratios from 2003 to 2009 as derived from SCIAMACHY: Trends and variability, *J. Geophys. Res.*, doi:10.1029/2010JD014849, 2011.

Feng, L., Palmer, P. I., Zhu, S. et al. Tropical methane emissions explain large fraction of recent changes in global atmospheric methane growth rate. *Nat Commun* 13, 1378, <https://doi.org/10.1038/s41467-022-28989-z>, 2022.

Frankenberg, C., Product User Guide (PUG) for the IMAP-DOAS XCH<sub>4</sub> SCIAMACHY Data Products, version 1, ESA Climate Change Initiative (CCI) GHG-CCI project, 13 Dec. 2012, 2012.

Fraser, A., Palmer, P. I., Feng, L., et al., Estimating regional methane surface fluxes: the relative importance of surface and GOSAT mole fraction measurements, *Atmos. Chem. Phys.*, 13, 5697-5713, doi:10.5194/acp-13-5697-2013, 2013.

Fraser, A., Palmer, P. I., Feng, L. et al., Estimating regional fluxes of CO<sub>2</sub> and CH<sub>4</sub> using space-borne observations of XCH<sub>4</sub>:XCO<sub>2</sub>, *Atmos. Chem. Phys.*, 14, 12883-12895, doi:10.5194/acp-14-12883-2014, 2014.

**Climate Assessment Report (CAR)  
for Climate Research Data Package 9 (CRDP#9)**

Version 2.1

of the Essential Climate Variable (ECV)  
Greenhouse Gases (GHG)

6 February 2025

Friedl, M. A., Strahler, A. H., and Hodges, J.: ISLSCP II MODIS (Collection 4) IGBP Land Cover, 2000–2001, in: ISLSCP Initiative II Collection, Data set, edited by: Hall, F. G., Collatz, G., Meeson, B., Los, S., Brown de Colstoun, E., and Landis, D., Oak Ridge National Laboratory Distributed Active Archive Center, Oak Ridge, Tennessee, USA, doi:10.3334/ORNLDAPAC/96

Friedlingstein, P., O’Sullivan, M., Jones, M. W., Andrew, R. M., Bakker, D. C. E., Hauck, J., Landschützer, P., Le Quéré, C., Luijkx, I. T., Peters, G. P., Peters, W., Pongratz, J., Schwingshackl, C., Sitch, S., Canadell, J. G., Ciais, P., Jackson, R. B., Alin, S. R., Anthoni, P., Barbero, L., Bates, N. R., Becker, M., Bellouin, N., Decharme, B., Bopp, L., Brasika, I. B. M., Cadule, P., Chamberlain, M. A., Chandra, N., Chau, T.-T.-T., Chevallier, F., Chini, L. P., Cronin, M., Dou, X., Enyo, K., Evans, W., Falk, S., Feely, R. A., Feng, L., Ford, D. J., Gasser, T., Ghattas, J., Gkritzalis, T., Grassi, G., Gregor, L., Gruber, N., Gürses, Ö., Harris, I., Hefner, M., Heinke, J., Houghton, R. A., Hurtt, G. C., Iida, Y., Ilyina, T., Jacobson, A. R., Jain, A., Jarníková, T., Jersild, A., Jiang, F., Jin, Z., Joos, F., Kato, E., Keeling, R. F., Kennedy, D., Klein Goldewijk, K., Knauer, J., Korsbakken, J. I., Körtzinger, A., Lan, X., Lefèvre, N., Li, H., Liu, J., Liu, Z., Ma, L., Marland, G., Mayot, N., McGuire, P. C., McKinley, G. A., Meyer, G., Morgan, E. J., Munro, D. R., Nakaoka, S.-I., Niwa, Y., O’Brien, K. M., Olsen, A., Omar, A. M., Ono, T., Paulsen, M., Pierrot, D., Pocock, K., Poulter, B., Powis, C. M., Rehder, G., Resplandy, L., Robertson, E., Rödenbeck, C., Rosan, T. M., Schwinger, J., Séférian, R., Smallman, T. L., Smith, S. M., Sospedra-Alfonso, R., Sun, Q., Sutton, A. J., Sweeney, C., Takao, S., Tans, P. P., Tian, H., Tilbrook, B., Tsjino, H., Tubiello, F., van der Werf, G. R., van Ooijen, E., Wanninkhof, R., Watanabe, M., Wimart-Rousseau, C., Yang, D., Yang, X., Yuan, W., Yue, X., Zaehle, S., Zeng, J., and Zheng, B.: Global Carbon Budget 2023, *Earth Syst. Sci. Data*, 15, 5301–5369, <https://doi.org/10.5194/essd-15-5301-2023>, 2023.

Fuentes Andrade, B., Buchwitz, M., Reuter, M., Bovensmann, H., Richter, A., Boesch, H., and Burrows, J. P.: A method for estimating localized CO<sub>2</sub> emissions from co-located satellite XCO<sub>2</sub> and NO<sub>2</sub> images, *EGUsphere* [preprint], <https://doi.org/10.5194/egusphere-2023-2085>, 2023.

Gatti, L. V., Gloor, M., Miller, J. B., Doughty, C. E., Malhi, Y., Domingues, L. G., Basso, L. S., Martinewski, A., Correia, C. S. C., Borges, V. F., Freitas, S., Braz, R., Anderson, L. O., Rocha, H., Grace, J., Philips, O. L., and Lloyd, J.: Drought sensitivity of Amazonian carbon balance revealed by atmospheric measurements, *Nature*, 506(7486), 76–80, doi:10.1038/nature12957, 2014

Gao, M., Xing, Z., Vollrath, C. et al. Global observational coverage of onshore oil and gas methane sources with TROPOMI. *Sci Rep* 13, 16759, <https://doi.org/10.1038/s41598-023-41914-8>, 2023.

Cooperative Global Atmospheric Data Integration Project. (2020). *Multi-laboratory compilation of atmospheric carbon dioxide data for the period 1957-2019; obspack\_co2\_1\_GLOBALVIEWplus\_v6.0\_2020\_09\_11* [Data set]. NOAA Earth System Research Laboratory, Global Monitoring Division. <https://doi.org/10.25925/20200903>

Guerlet, S., Basu, S., Butz, A., et al., Reduced carbon uptake during the 2010 Northern Hemisphere summer from GOSAT, *Geophys. Res. Lett.*, doi: 10.1002/grl.50402, 2013.

	ESA Climate Change Initiative (CCI+)	Page 41
	<b>Climate Assessment Report (CAR)</b> for Climate Research Data Package 9 (CRDP#9)	Version 2.1
	of the Essential Climate Variable (ECV) Greenhouse Gases (GHG)	6 February 2025

Gurney, K.R., et al.: Towards robust regional estimates of CO<sub>2</sub> sources and sinks using atmospheric transport models. *Nature*, 415:6872, 626-630, 2002.

Harris, I., Jones, P.D., Osborn, T.J. and Lister, D.H., Updated high-resolution grids of monthly climatic observations – the CRU TS3.10 Dataset. *Int. J. Climatol.* doi: 10.1002/joc.3711, 2013

Haverd, V., Raupach, M. R., Briggs, P. R., J. G. Canadell., Davis, S. J., Law, R. M., Meyer, C. P., Peters, G. P., Pickett-Heaps, C., and Sherman, B.: The Australian terrestrial carbon budget, *Biogeosciences*, 10, 851-869, doi:10.5194/bg-10-851-2013, 2013.

Hayman, G. D., O'Connor, F. M., Dalvi, et al., Comparison of the HadGEM2 climate-chemistry model against in-situ and SCIAMACHY atmospheric methane data, *Atmos. Chem. Phys.*, 14, 13257-13280, doi:10.5194/acp-14-13257-2014, 2014.

Heimann, M.: The global atmospheric tracer model TM2, Technical Report No. 10, Max-Planck-Institut für Meteorologie, Hamburg, Germany. 1995

Heimann, M., G. Esser, A. Haxeltine, J. Kaduk, D.W. Kicklighter, W. Knorr, G. H. Kohlmaier, A. D. McGuire, J. Melillo, B. Moore, et al., Evaluation of terrestrial carbon cycle models through simulations of the seasonal cycle of atmospheric CO<sub>2</sub>: First results of a model intercomparison study, *Global Biogeochemical Cycles*, 12, 1–24, 1998.

Heimann, M. and S. Körner: The global atmospheric tracer model TM3. In: Max-Planck-Institut für Biogeochemie (Eds.): Technical Report. Vol. 5. Max-Planck-Institut für Biogeochemie, Jena. pp. 131, 2003.

Heymann, J., Schneising, O., Reuter, M., et al., SCIAMACHY WFM-DOAS XCO<sub>2</sub>: comparison with CarbonTracker XCO<sub>2</sub> focusing on aerosols and thin clouds, *Atmos. Meas. Tech.*, 5, 1935-1952, 2012.

Hourdin, F., Rio, C., Grandpeix, J.-Y., Madeleine, J.-B., Cheruy, F., Rochetin, N., et al. (2020). LMDZ6A: The atmospheric component of the IPSL climate model with improved and better tuned physics. *Journal of Advances in Modeling Earth Systems*, 12(7), e2019MS001892. <https://doi.org/10.1029/2019MS001892>

Houweling, S., et al.: The importance of transport model uncertainties for the estimation of CO<sub>2</sub> sources and sinks using satellite measurements. *Atmos. Chem. Phys.*, 10, 9981-9992, doi:10.5194/acp-10-9981-2010, 2010.

Houweling, S., M. Krol, P. Bergamaschi, C. Frankenberg, E. J. Dlugokencky, I. Morino, J. Notholt, V. Sherlock, D. Wunch, V. Beck, C. Gerbig, H. Chen, E. A. Kort, T. Röckmann and I. Aben, A multi-year methane inversion using SCIAMACHY, accounting for systematic errors using TCCON measurements, *Atmos. Chem. Phys.*, 14, 3991–4012, doi:10.5194/acp-14-3991-2014, 2014.

Houweling, S., D. Baker, S. Basu, H. Boesch, A. Butz, F. Chevallier, F. Deng, E. Dlugokencky, L. Feng, A. Ganshin, O. P. Hasekamp, D. Jones, S. Maksyutov, J. Marshall, T. Oda, C. O'Dell, S. Oshchepkov, P.

	ESA Climate Change Initiative (CCI+)	Page 42
	<b>Climate Assessment Report (CAR)</b> <b>for Climate Research Data Package 9 (CRDP#9)</b>	Version 2.1
	of the Essential Climate Variable (ECV) Greenhouse Gases (GHG)	6 February 2025

Paul, P. Peylin, Z. Poussi, F. Reum, H. Takagi, Y. Yoshida, R. Zhuravlev, An inter-comparison of inverse models for estimating sources and sinks of CO<sub>2</sub> using GOSAT measurements. *J. Geophys. Res. Atmos.*, 120, 5253–5266, doi:10.1002/2014JD022962, 2015.

Hu, H., Hasekamp, O., Butz, A., Galli, A., Landgraf, J., Aan de Brugh, J., Borsdorff, T., Scheepmaker, R., and Aben, I.: The operational methane retrieval algorithm for TROPOMI, *Atmos. Meas. Tech.*, 9, 5423–5440, <https://doi.org/10.5194/amt-9-5423-2016>, 2016.

Kirschke, S., Bousquet, P., Ciais, P., et al., Three decades of global methane sources and sinks, *Nat. Geosci.*, 6, 813–823, doi:10.1038/ngeo1955, 2013.

Kort, E. A., Frankenberg, C., Costigan, K. R., et al., Four corners: The largest US methane anomaly viewed from space, *Geophys. Res. Lett.*, 41, doi:10.1002/2014GL061503, 2014.

Krisna, T. C., et al.: ESA Climate Change Initiative “Plus” (CCI+) Product User Guide (PUG) Version 3.0 for the RemoTeC XCO<sub>2</sub> GOSAT-2 SRON Full-Physics Product (CO<sub>2</sub>\_GO<sub>2</sub>\_SRFP) Version 2.0.0, Technical Report, pp. 21, [https://www.iup.uni-bremen.de/carbon\\_ghg/docs/GHG-CClplus/CRDP7/PUGv3\\_GHG-CCI\\_CO2\\_GO2\\_SRFP\\_v2.0.0.pdf](https://www.iup.uni-bremen.de/carbon_ghg/docs/GHG-CClplus/CRDP7/PUGv3_GHG-CCI_CO2_GO2_SRFP_v2.0.0.pdf), 2022a.

Krisna, T. C., et al.: ESA Climate Change Initiative “Plus” (CCI+) Product User Guide (PUG) Version 3.0 for the RemoTeC XCH<sub>4</sub> GOSAT-2 PROXY Product (CH<sub>4</sub>\_GO<sub>2</sub>\_SRPR) version 2.0.0, [https://www.iup.uni-bremen.de/carbon\\_ghg/docs/GHG-CClplus/CRDP7/PUGv3\\_GHG-CCI\\_CH4\\_GO2\\_SRPR\\_v2.0.0.pdf](https://www.iup.uni-bremen.de/carbon_ghg/docs/GHG-CClplus/CRDP7/PUGv3_GHG-CCI_CH4_GO2_SRPR_v2.0.0.pdf), 2022b.

Krol, M. C., S. Houweling, B. Bregman, M. van den Broek, A. Segers, P. van Velthoven, W. Peters, F. Dentener, and P. Bergamaschi, The two-way nested global chemistry-transport zoom model TM5: algorithm and applications, *Atmos. Chem. Phys.*, 5, 417-432, 2005.

Lan, X., K.W. Thoning, and E.J. Dlugokencky: Trends in globally-averaged CH<sub>4</sub>, N<sub>2</sub>O, and SF<sub>6</sub> determined from NOAA Global Monitoring Laboratory measurements. Version 2023-01, <https://doi.org/10.15138/P8XG-AA10>, 2022.

Lauvaux, T., Giron, C., Mazzolini, M. et al., Global assessment of oil and gas methane ultra-emitters. *Science* 375, 557-561 doi:10.1126/science.abj4351, 2022.

Liang, R., Zhang, Y., Chen, W., Zhang, P., Liu, J., Chen, C., Mao, H., Shen, G., Qu, Z., Chen, Z., Zhou, M., Wang, P., Parker, R. J., Boesch, H., Lorente, A., Maasackers, J. D., and Aben, I.: East Asian methane emissions inferred from high-resolution inversions of GOSAT and TROPOMI observations: a comparative and evaluative analysis, *Atmos. Chem. Phys.*, 23, 8039–8057, <https://doi.org/10.5194/acp-23-8039-2023>, 2023.

Lindqvist, H., C. W. O'Dell, S. Basu, H. Boesch, F. Chevallier, N. Deutscher, L. Feng, B. Fisher, F. Hase, M. Inoue, R. Kivi, I. Morino, P. I. Palmer, R. Parker, M. Schneider, R. Sussmann, and Y. Yoshida, Does

	ESA Climate Change Initiative (CCI+)	Page 43
	<b>Climate Assessment Report (CAR) for Climate Research Data Package 9 (CRDP#9)</b>	Version 2.1
	of the Essential Climate Variable (ECV) Greenhouse Gases (GHG)	6 February 2025

GOSAT capture the true seasonal cycle of carbon dioxide?; *Atmos. Chem. Phys.*, 15, 13023-13040, doi:10.5194/acp-15-13023-2015, 2015.

Liu, J., K. W. Bowman, D. Schimel, N. C. Parazoo, Z. Jiang, M. Lee, A. A. Bloom, D. Wunch, C. Frankenberg, Y. Sun, C. W. O'Dell, K. R. Gurney, D. Menemenlis, M. Girerach, D. Crisp, and A. Eldering, Contrasting carbon cycle responses of the tropical continents to the 2015–2016 El Niño. *Science* 358, doi:10.1126/science.aam5690, 2017.

R. Gurney, D. Menemenlis, M. Girerach, D. Crisp, and A. Eldering, Contrasting carbon cycle responses of the tropical continents to the 2015–2016 El Niño. *Science* 358, eaam5690 (2017) Lorente, A., Borsdorff, T., Butz, A., Hasekamp, O., van de Brugh, J., Schneider, A., Wu, L., Hase, F., Kivi, R., Wunch, D., Pollard, D. F., Shiomi, K., Deutscher, N. M., Velasco, V. A., Roehl, C. M., Wennberg, P. O., Warneke, T., and Landgraf, J.: Methane retrieved from TROPOMI: improvement of the data product and validation of the first 2 years of measurements, *Atmos. Meas. Tech.*, 14, 665–684, <https://doi.org/10.5194/amt-14-665-2021>, 2021.

Lu, X., Jacob, D. J., Wang, H., Maasackers, J. D., Zhang, Y., Scarpelli, T. R., Shen, L., Qu, Z., Sulprizio, M. P., Nesser, H., Bloom, A. A., Ma, S., Worden, J. R., Fan, S., Parker, R. J., Boesch, H., Gautam, R., Gordon, D., Moran, M. D., Reuland, F., Villasana, C. A. O., and Andrews, A.: Methane emissions in the United States, Canada, and Mexico: evaluation of national methane emission inventories and 2010–2017 sectoral trends by inverse analysis of in situ (GLOBALVIEWplus CH<sub>4</sub> ObsPack) and satellite (GOSAT) atmospheric observations, *Atmos. Chem. Phys.*, 22, 395–418, <https://doi.org/10.5194/acp-22-395-2022>, 2022.

Lunt, M. F., Palmer, P. I., Feng, L., Taylor, C. M., Boesch, H., and Parker, R. J.: An increase in methane emissions from tropical Africa between 2010 and 2016 inferred from satellite data, *Atmos. Chem. Phys.*, 19, 14721–14740, <https://doi.org/10.5194/acp-19-14721-2019>, 2019.

Maasackers, J., Omara, M., Gautam, R. et al., Reconstructing and quantifying methane emissions from the full duration of a 38-day natural gas well blowout using space-based observations. *Remote Sensing of Environment*. 270. 112755, doi:10.1016/j.rse.2021.112755, 2021.

Maasackers JD, Varon DJ, Elfarsdóttir A, McKeever J, Jervis D, Mahapatra G, Pandey S, Lorente A, Borsdorff T, Foorthuis LR, Schuit BJ, Tol P, van Kempen TA, van Hees R, Aben I. Using satellites to uncover large methane emissions from landfills. *Sci Adv.*, Aug 12;8(32). doi: 10.1126/sciadv.abn9683, 2022.

Ma, X., A. Huete, J. Cleverly, D. Eamus, F. Chevallier, J. Joiner, B. Poulter, Y. Zhang, L. Guanter, W. Meyer, Z. Xie, G. Ponce-Campos: Drought rapidly disseminates the 2011 large CO<sub>2</sub> uptake in semi-arid Australia. *Scientific Reports*, 6. doi: 10.1038/srep37747, 2016.

Mäder, J. A., J. Staehelin, D. Brunner, W. A. Stahel, I. Wohltmann, and T. Peter, Statistical modeling of total ozone: Selection of appropriate explanatory variables, *J. Geophys. Res.*, 112, D11108, doi:10.1029/2006JD007694, 2007.

	ESA Climate Change Initiative (CCI+)	Page 44
	<b>Climate Assessment Report (CAR)</b> for Climate Research Data Package 9 (CRDP#9)	Version 2.1
	of the Essential Climate Variable (ECV) Greenhouse Gases (GHG)	6 February 2025

Meirink, J. F., P. Bergamaschi, and M. Krol: Four-dimensional variational data assimilation for inverse modelling of atmospheric methane emissions: Method and comparison with synthesis inversion, *Atmos. Chem. Phys.*, 8, 6341–6353, 2008.

Monteil, G., Houweling, S., Butz, A., et al., Comparison of CH<sub>4</sub> inversions based on 15 months of GOSAT and SCIAMACHY observations, *J. Geophys. Res.*, doi: 10.1002/2013JD019760, Vol 118, Issue 20, 11807–11823, 2013.

Nassar, R., Hill, T. G., McLinden, C. A., Wunch, D., Jones, D. B. A., & Crisp, D., Quantifying CO<sub>2</sub> emissions from individual power plants from space. *Geophysical Research Letters*, 44, 10,045–10,053. <https://doi.org/10.1002/2017GL074702>, 2017.

O'Dell, C. W., Connor, B., Bösch, H., O'Brien, D., Frankenberg, C., Castano, R., Christi, M., Eldering, D., Fisher, B., Gunson, M., McDuffie, J., Miller, C. E., Natraj, V., Oyafuso, F., Polonsky, I., Smyth, M., Taylor, T., Toon, G. C., Wennberg, P. O., and Wunch, D.: The ACOS CO<sub>2</sub> retrieval algorithm – Part 1: Description and validation against synthetic observations, *Atmos. Meas. Tech.*, 5, 99–121, doi:10.5194/amt-5-99-2012, 2012.

O'Dell, C. W., Eldering, A., Wennberg, P. O., Crisp, D., Gunson, M. R., Fisher, B., Frankenberg, C., Kiel, M., Lindqvist, H., Mandrake, L., Merrelli, A., Natraj, V., Nelson, R. R., Osterman, G. B., Payne, V. H., Taylor, T. E., Wunch, D., Drouin, B. J., Oyafuso, F., Chang, A., McDuffie, J., Smyth, M., Baker, D. F., Basu, S., Chevallier, F., Crowell, S. M. R., Feng, L., Palmer, P. I., Dubey, M., García, O. E., Griffith, D. W. T., Hase, F., Iraci, L. T., Kivi, R., Morino, I., Notholt, J., Ohyama, H., Petri, C., Roehl, C. M., Sha, M. K., Strong, K., Sussmann, R., Te, Y., Uchino, O., and Velasco, V. A.: Improved retrievals of carbon dioxide from Orbiting Carbon Observatory-2 with the version 8 ACOS algorithm, *Atmos. Meas. Tech.*, 11, 6539–6576, <https://doi.org/10.5194/amt-11-6539-2018>, 2018.

Oda, T., and Maksyutov, S.: A very high-resolution (1 km×1 km) global fossil fuel CO<sub>2</sub> emission inventory derived using a point source database and satellite observations of nighttime lights, *Atmos. Chem. Phys.*, 11, 543–556, doi:10.5194/acp-11-543-2011, 2011.

Olivier, J. G. J., van Aardenne, J. A., Dentener, F., Ganzeveld, L., and Peters, J. A. H. W.: Recent trends in global greenhouse gas emissions: regional trends and spatial distribution of key sources, in: *Non-CO<sub>2</sub> Greenhouse Gases (NCGG-4)*, edited by: van Amstel, A., Millpress, Rotterdam, 325–330, 2005.

Olivier, J. G. J., Janssens-Maenhout, G., and Peters, J. A. H. W., Trends in global CO<sub>2</sub> emissions, 2012 Report, PBL Netherlands Environmental Assessment Agency, The Hague, Joint Research Centre, Ispra, ISBN 978-92-79-25381-2, 2012.

Oshchepkov, S., A. Bril, T. Yokota, et al., Effects of atmospheric light scattering on spectroscopic observations of greenhouse gases from space. Part 2: Algorithm intercomparison in the GOSAT data processing for CO<sub>2</sub> retrievals over TCCON sites, *J. Geophys. Res.*, 118, 1493–1512, doi:10.1002/jgrd.50146, 2013.

**Climate Assessment Report (CAR)  
for Climate Research Data Package 9 (CRDP#9)**

Version 2.1

of the Essential Climate Variable (ECV)  
Greenhouse Gases (GHG)

6 February 2025

Osterman, G., and team (2022). Orbiting Carbon Observatory-2 & 3 (OCO-2 & OCO-3) – Data Product User’s Guide, Operational Level 2 Lite Files – Version 2.0 – Revision A – July 5, 2022 – Data Release: 11 (OCO-2), 10/10.4 (OCO-3), [https://docserver.gesdisc.eosdis.nasa.gov/public/project/OCO/OCO2\\_V11\\_OCO3\\_V10\\_DUG.pdf](https://docserver.gesdisc.eosdis.nasa.gov/public/project/OCO/OCO2_V11_OCO3_V10_DUG.pdf)

Pandey, S., Houweling, S., Krol, M., Aben, I., Chevallier, F., Dlugokencky, E. J., Gatti, L. V., Gloor, M., Miller, J. B., Detmers, R., Machida, T., and Röckmann, T.: Inverse modeling of GOSAT-retrieved ratios of total column CH<sub>4</sub> and CO<sub>2</sub> for 2009 and 2010, *Atmos. Chem. Phys. Discuss.*, doi:10.5194/acp-2016-77, in review, 2016.

Parazoo, N. C., Bowman, K., Frankenberg, C., et al., Interpreting seasonal changes in the carbon balance of southern Amazonia using measurements of XCO<sub>2</sub> and chlorophyll fluorescence from GOSAT, *Geophys. Res. Lett.*, 40, 2829–2833, doi:10.1002/grl.50452, 2013.

Parker, R., Boesch, H., Cogan, A., et al., Methane Observations from the Greenhouse gases Observing SATellite: Comparison to ground-based TCCON data and Model Calculations, *Geophys. Res. Lett.*, doi:10.1029/2011GL047871, 2011.

Parker, R., Boesch, H., McNorton, J., et al. : Evaluating year-to-year anomalies in tropical wetland methane emissions using satellite CH<sub>4</sub> observations, *Remote Sensing of Environment*, 211, 261–275, doi:10.1016/j.rse.2018.02.011, 2018.

Peng, S., Lin, X., Thompson, R.L. et al. Wetland emission and atmospheric sink changes explain methane growth in 2020. *Nature* 612, 477–482, doi: 10.1038/s41586-022-05447-w, 2022.

Peters, W., Jacobson, A. R., Sweeney, C., et al.: An atmospheric perspective on North American carbon dioxide exchange: CarbonTracker, *Proceedings of the National Academy of Sciences (PNAS)* of the United States of America, 27 Nov. 2007, 104(48), 18925-18930, 2007.

Peylin, P., Law, R. M., Gurney, et al., Global atmospheric carbon budget: results from an ensemble of atmospheric CO<sub>2</sub> inversions, *Biogeosciences*, 10, 6699–6720, doi:10.5194/bg-10-6699-2013, URL <http://www.biogeosciences.net/10/6699/2013/>, 2013.

Pinty, B., G. Janssens-Maenhout, M. Dowell, H. Zunker, T. Brunhes, P. Ciais, D. Dee, H. Denier van der Gon, H. Dolman, M. Drinkwater, R. Engelen, M. Heimann, K. Holmlund, R. Husband, A. Kentarchos, Y. Meijer, P. Palmer and M. Scholze (2017) An operational anthropogenic CO<sub>2</sub> emissions monitoring & verification support capacity - Baseline requirements, Model components and functional architecture, doi:10.2760/39384, European Commission Joint Research Centre, EUR 28736 EN.

Poulter, B., Frank, D., Ciais, P., Myneni, R. B., Andela, N., Bi, J., Broquet, G. Canadell, J.G. Chevallier, F. Liu, Y. Y., Running, S. W., Sitch, S., and van der Werf, G. R.: Contribution of semi-arid ecosystems to interannual variability of the global carbon cycle. *Nature*, doi:10.1038/nature13376, 2014.

	ESA Climate Change Initiative (CCI+)	Page 46
	<b>Climate Assessment Report (CAR)</b> <b>for Climate Research Data Package 9 (CRDP#9)</b>	Version 2.1
	of the Essential Climate Variable (ECV) Greenhouse Gases (GHG)	6 February 2025

Prather, M.: Interactive comment on “Carbon dioxide and climate impulse response functions for the computation of greenhouse gas metrics: a multi-model analysis” by F. Joos et al, *Atmos. Chem. Phys. Discuss.*, 12, C8465–C8470, [www.atmos-chem-phys-discuss.net/12/C8465/2012/](http://www.atmos-chem-phys-discuss.net/12/C8465/2012/), 2012.

Remaud, M., Chevallier, F., Cozic, A., Lin, X., and Bousquet, P.: On the impact of recent developments of the LMDz atmospheric general circulation model on the simulation of CO<sub>2</sub> transport, *Geosci. Model Dev.*, 11, 4489–4513, <https://doi.org/10.5194/gmd-11-4489-2018>, 2018.

Reuter, M., Bovensmann, H., Buchwitz, M., et al., Retrieval of atmospheric CO<sub>2</sub> with enhanced accuracy and precision from SCIAMACHY: Validation with FTS measurements and comparison with model results, *J. Geophys. Res.*, 116, D04301, doi:10.1029/2010JD015047, 2011.

Reuter, M., Boesch, H., Bovensmann, H., et al., A joint effort to deliver satellite retrieved atmospheric CO<sub>2</sub> concentrations for surface flux inversions: the ensemble median algorithm EMMA, *Atmos. Chem. Phys.*, 13, 1771-1780, 2013.

Reuter, M., M. Buchwitz, M. Hilker, et al., Satellite-inferred European carbon sink larger than expected, *Atmos. Chem. Phys.*, 14, 13739-13753, doi:10.5194/acp-14-13739-2014, 2014a.

Reuter, M., M. Buchwitz, A. Hilboll, et al., Decreasing emissions of NO<sub>x</sub> relative to CO<sub>2</sub> in East Asia inferred from satellite observations, *Nature Geoscience*, 28 Sept. 2014, doi:10.1038/ngeo2257, pp.4, 2014b.

Reuter, M.: ESA Climate Change Initiative (CCI) Product User Guide version 4 (PUGv4) for the XCO<sub>2</sub> SCIAMACHY Data Product BESD for the Essential Climate Variable (ECV): Greenhouse Gases (GHG), 31 August 2016, 2016a.

Reuter, M., M. Hilker, O. Schneising, M. Buchwitz, J. Heymann ESA Climate Change Initiative (CCI) Comprehensive Error Characterisation Report: BESD full-physics retrieval algorithm for XCO<sub>2</sub> for the Essential Climate Variable (ECV) Greenhouse Gases (GHG) Version 2.0, revision 1. 2016b.

Reuter, M., M. Buchwitz, M. Hilker, J. Heymann, H. Bovensmann, J. P. Burrows, S. Houweling, Y. Y. Liu, R. Nassar, F. Chevallier, et al., How much CO<sub>2</sub> is taken up by the European terrestrial biosphere?, *Bulletin of the American Meteorological Society*, 0(0), doi:10.1175/BAMS-D-15-00310.1, 2016c.

Reuter, M., M. Buchwitz, O. Schneising, S. Noel, V. Rozanov, H. Bovensmann, J. P. Burrows, A Fast Atmospheric Trace Gas Retrieval for Hyperspectral Instruments Approximating Multiple Scattering - Part 1: Radiative Transfer and a Potential OCO-2 XCO<sub>2</sub> Retrieval Setup, *Remote Sens.*, 9, 1159, doi:10.3390/rs9111159, 2017a.

Reuter, M., M. Buchwitz, O. Schneising, S. Noel, H. Bovensmann, J. P. Burrows, A Fast Atmospheric Trace Gas Retrieval for Hyperspectral Instruments Approximating Multiple Scattering - Part 2: Application to XCO<sub>2</sub> Retrievals from OCO-2, *Remote Sens.*, 9, 1102, doi:10.3390/rs9111102, 2017b.

**Climate Assessment Report (CAR)  
for Climate Research Data Package 9 (CRDP#9)**

Version 2.1

of the Essential Climate Variable (ECV)  
Greenhouse Gases (GHG)

6 February 2025

Reuter, M., Buchwitz, M., Schneising, O., Krautwurst, S., O'Dell, C. W., Richter, A., Bovensmann, H., and Burrows, J. P.: Towards monitoring localized CO<sub>2</sub> emissions from space: co-located regional CO<sub>2</sub> and NO<sub>2</sub> enhancements observed by the OCO-2 and S5P satellites, *Atmos. Chem. Phys.*, 19, 9371–9383, <https://doi.org/10.5194/acp-19-9371-2019>, 2019.

Reuter, M., Buchwitz, M., Schneising, O., Noël, S., Bovensmann, H., Burrows, J. P., Boesch, H., Di Noia, A., Anand, J., Parker, R. J., Somkuti, P., Wu, L., Hasekamp, O. P., Aben, I., Kuze, A., Suto, H., Shiomi, K., Yoshida, Y., Morino, I., Crisp, D., O'Dell, C. W., Notholt, J., Petri, C., Warneke, T., Velazco, V. A., Deutscher, N. M., Griffith, D. W. T., Kivi, R., Pollard, D. F., Hase, F., Sussmann, R., Té, Y. V., Strong, K., Roche, S., Sha, M. K., De Mazière, M., Feist, D. G., Iraci, L. T., Roehl, C. M., Retscher, C., and Schepers, D.: Ensemble-based satellite-derived carbon dioxide and methane column-averaged dry-air mole fraction data sets (2003–2018) for carbon and climate applications, *Atmos. Meas. Tech.*, 13, 789–819, <https://doi.org/10.5194/amt-13-789-2020>, 2020.

Rödenbeck, C.: Estimating CO<sub>2</sub> sources and sinks from atmospheric mixing ratio measurements using a global inversion of atmospheric transport, Tech. Rep. 6, Max Planck Institute for Biogeochemistry, Jena, Germany, 2005.

Ross, A. N., Wooster, M. J., Boesch, H., Parker, R., First satellite measurements of carbon dioxide and methane emission ratios in wildfire plumes, *Geophys. Res. Lett.*, 40, 1-5, doi:10.1002/grl.50733, 2013.

Scarle, J. D., Studies in astronomical time series analysis. III. Fourier transforms, autocorrelation functions and cross-correlation functions of unevenly spaced data. *Astrophys. J.*, 343, 874–887, 1989.

Schneising, O., Buchwitz, M., Reuter, M., et al., Long-term analysis of carbon dioxide and methane column-averaged mole fractions retrieved from SCIAMACHY, *Atmos. Chem. Phys.*, 11, 2881-2892, 2011.

Schneising, O., J. Heymann, M. Buchwitz, M. Reuter, H. Bovensmann, and J. P. Burrows, Anthropogenic carbon dioxide source areas observed from space: assessment of regional enhancements and trends, *Atmos. Chem. Phys.*, 13, 2445-2454, 2013.

Schneising, O., M. Reuter, M. Buchwitz, J. Heymann, H. Bovensmann, and J. P. Burrows, Terrestrial carbon sink observed from space: variation of growth rates and seasonal cycle amplitudes in response to interannual surface temperature variability, *Atmos. Chem. Phys.*, 14, 133-141, 2014a.

Schneising, O., J. P. Burrows, R. R. Dickerson, M. Buchwitz, M. Reuter, H. Bovensmann, Remote sensing of fugitive methane emissions from oil and gas production in North American tight geologic formations, *Earth's Future*, 2, DOI: 10.1002/2014EF000265, pp. 11, 2014b.

Schneising, O., Buchwitz, M., Reuter, M., Bovensmann, H., Burrows, J. P., Borsdorff, T., Deutscher, N. M., Feist, D. G., Griffith, D. W. T., Hase, F., Hermans, C., Iraci, L. T., Kivi, R., Landgraf, J., Morino, I., Notholt, J., Petri, C., Pollard, D. F., Roche, S., Shiomi, K., Strong, K., Sussmann, R., Velazco, V. A.,

	ESA Climate Change Initiative (CCI+)	Page 48
	<b>Climate Assessment Report (CAR)</b> <b>for Climate Research Data Package 9 (CRDP#9)</b>	Version 2.1
	of the Essential Climate Variable (ECV) Greenhouse Gases (GHG)	6 February 2025

Warneke, T., and Wunch, D.: A scientific algorithm to simultaneously retrieve carbon monoxide and methane from TROPOMI onboard Sentinel-5 Precursor, *Atmos. Meas. Tech.*, 12, 6771–6802, <https://doi.org/10.5194/amt-12-6771-2019>, 2019.

Schneising, O., Buchwitz, M., Reuter, M., Vanselow, S., Bovensmann, H., and Burrows, J. P.: Remote sensing of methane leakage from natural gas and petroleum systems revisited, *Atmos. Chem. Phys.*, 20, 9169–9182, <https://doi.org/10.5194/acp-20-9169-2020>, 2020.

Schuit, B. J., Maasackers, J. D., Bijl, P., Mahapatra, G., van den Berg, A.-W., Pandey, S., Lorente, A., Borsdorff, T., Houweling, S., Varon, D. J., McKeever, J., Jervis, D., Girard, M., Irakulis-Loitxate, I., Gorroño, J., Guanter, L., Cusworth, D. H., and Aben, I.: Automated detection and monitoring of methane super-emitters using satellite data, *Atmos. Chem. Phys.*, 23, 9071–9098, <https://doi.org/10.5194/acp-23-9071-2023>, 2023.

Schuldt et al., Multi-laboratory compilation of atmospheric methane data for the period 1983-2022; obspack\_ch4\_1\_GLOBALVIEWplus\_v6.0\_2023-12-01; NOAA Earth System Research Laboratory, Global Monitoring Laboratory, <http://doi.org/10.25925/20231001>, 2023.

Schuldt et al., Multi-laboratory compilation of atmospheric methane data for the period 2023-2024; obspack\_ch4\_1\_NRT\_v6.2\_2024-06-27; NOAA Earth System Research Laboratory, Global Monitoring Laboratory, <http://doi.org/10.25925/20240612>, 2024.

Schulze, E. D., Luyssaert, S., Ciais, P., Freibauer, A., Janssens, I. A., Soussana, J. F., Smith, P., Grace, J., Levin, I., Tiruchittampalam, B., Heimann, M., Dolman, A. J., Valentini, R., Bousquet, P., Peylin, P., Peters, W., Rodenbeck, C., Etiope, G., Vuichard, N., Wattenbach, M., Nabuurs, G. J., Poussi, Z., Nieschulze, J., Gash, J. H., and Team, C.: Importance of methane and nitrous oxide emissions for Europe's terrestrial greenhouse gas balance, *Nat. Geosci.*, 2, 842–850, 2009.

Shen, L., Jacob, D.J., Gautam, R. et al. National quantifications of methane emissions from fuel exploitation using high resolution inversions of satellite observations. *Nat Commun* 14, 4948, [doi:10.1038/s41467-023-40671-6](https://doi.org/10.1038/s41467-023-40671-6), 2023.

Shindell, D. T., O. Pechony, A. Voulgarakis, et al., Interactive ozone and methane chemistry in GISS-E2 historical and future climate simulations, *Atmos. Chem. Phys.*, 13, 2653–2689, doi:10.5194/acp-13-2653-2013, 2013.

Somkuti, P.: ESA Climate Change Initiative (CCI) Product User Guide version 4.0 (PUGv4.0) for the University of Leicester full-physics XCO<sub>2</sub> GOSAT data product (CO<sub>2</sub>\_GOS\_OCFP version 7) for the Essential Climate Variable (ECV): Greenhouse Gases (GHG), 31 August 2016, 2016.

Sussmann, R., Forster, F., Rettinger, M., and Bousquet, P.: Renewed methane increase for five years (2007–2011) observed by solar FTIR spectrometry, *Atmos. Chem. Phys.*, 12, 4885–4891, doi:10.5194/acp-12-4885-2012, 2012.

**Climate Assessment Report (CAR)  
for Climate Research Data Package 9 (CRDP#9)**

Version 2.1

of the Essential Climate Variable (ECV)  
Greenhouse Gases (GHG)

6 February 2025

Turner, A. J., Jacob, D. J., Wecht, K. J., Maasackers, J. D., Lundgren, E., Andrews, A. E., Biraud, S. C., Boesch, H., Bowman, K. W., Deutscher, N. M., Dubey, M. K., Griffith, D. W. T., Hase, F., Kuze, A., Notholt, J., Ohyama, H., Parker, R., Payne, V. H., Sussmann, R., Sweeney, C., Velazco, V. A., Warneke, T., Wennberg, P. O., and Wunch, D.: Estimating global and North American methane emissions with high spatial resolution using GOSAT satellite data, *Atmos. Chem. Phys.*, 15, 7049–7069, doi:10.5194/acp-15-7049-2015, 2015.

Varon, D. J., Jacob, D. J., Hmiel, B., Gautam, R., Lyon, D. R., Omara, M., Sulprizio, M., Shen, L., Pendergrass, D., Nesser, H., Qu, Z., Barkley, Z. R., Miles, N. L., Richardson, S. J., Davis, K. J., Pandey, S., Lu, X., Lorente, A., Borsdorff, T., Maasackers, J. D., and Aben, I.: Continuous weekly monitoring of methane emissions from the Permian Basin by inversion of TROPOMI satellite observations, *Atmos. Chem. Phys.*, 23, 7503–7520, <https://doi.org/10.5194/acp-23-7503-2023>, 2023.

Wanninkhof, R., Park, G. -H., Takahashi, T., Sweeney, C., Feely, R., Nojiri, Y., Gruber, N., Doney, S. C., McKinley, G. A., Lenton, A., Le Quéré, C., Heinze, C., Schwinger, J., Graven, H., and Khatiwala, S.: Global ocean carbon uptake: magnitude, variability and trends, *Biogeosciences*, 10, 1983–2000, doi:10.5194/bg-10-1983-2013, 2013.

van der Werf, G. R., Randerson, J. T., Giglio, L., Collatz, G. J., Mu, M., Kasibhatla, P. S., Morton, D. C., DeFries, R. S., Jin, Y., and van Leeuwen, T. T.: Global fire emissions and the contribution of deforestation, savanna, forest, agricultural, and peat fires (1997–2009), *Atmos. Chem. Phys.*, 10, 11707–11735, doi:10.5194/acp-10-11707-2010, 2010.

Vanselow, S., Schneising, O., Buchwitz, M., Reuter, M., Bovensmann, H., Boesch, H., and Burrows, J. P.: Automated detection of regions with persistently enhanced methane concentrations using Sentinel-5 Precursor satellite data, *Atmos. Chem. Phys.*, 24, 10441–10473, <https://doi.org/10.5194/acp-24-10441-2024>, 2024.

Wecht, K. J., D. J. Jacob, C. Frankenberg, Z. Jiang, and D. R. Blake (2014), Mapping of North American methane emissions with high spatial resolution by inversion of SCIAMACHY satellite data, *J. Geophys. Res. Atmos.*, 119, 7741–7756, doi:10.1002/2014JD021551.

Wunch, D., Toon, G. C., Blavier, J.-F., et al., The Total Carbon Column Observing Network, *Phil. Trans. R. Soc. A*, 369, 2087–2112, doi:10.1098/rsta.2010.0240, 2011.

Wunch, D., Wennberg, P. O., Toon, G. C. et al., A method for evaluating bias in global measurements of CO<sub>2</sub> total columns from space. *Atmos. Chem. Phys.*, 11, 12317–12337, 2011.

Yang, D. X., and Coauthors, 2021: A new TanSat XCO<sub>2</sub> global product towards climate studies. *Adv. Atmos. Sci.*, 38(1), 8–11, <https://doi.org/10.1007/s00376-020-0297-y>.

Yin, Y., Chevallier, F., Ciais, P., Bousquet, P., Saunois, M., Zheng, B., Worden, J., Bloom, A. A., Parker, R. J., Jacob, D. J., Dlugokencky, E. J., and Frankenberg, C.: Accelerating methane growth rate from

	ESA Climate Change Initiative (CCI+)	Page 50
	<b>Climate Assessment Report (CAR)</b> <b>for Climate Research Data Package 9 (CRDP#9)</b>	Version 2.1
	of the Essential Climate Variable (ECV) Greenhouse Gases (GHG)	6 February 2025

2010 to 2017: leading contributions from the tropics and East Asia, *Atmos. Chem. Phys.*, 21, 12631–12647, <https://doi.org/10.5194/acp-21-12631-2021>, 2021.

Yoshida, Y., Kikuchi, N., Morino, I., et al., Improvement of the retrieval algorithm for GOSAT SWIR XCO<sub>2</sub> and XCH<sub>4</sub> and their validation using TCCON data, *Atmos. Meas. Tech.*, 6, 1533–1547, doi:10.5194/amt-6-1533-2013, 2013.

Zhang, Y., Gautam, R., Pandey, S. et al., Quantifying methane emissions from the largest oil-producing basin in the United States from space. *Sci. Adv.* 6, 17, doi:10.1126/sciadv.aaz5120, 2020.

**END OF DOCUMENT**